Geochemistry Geophysics Geosystems G3
AN ELECTRONIC JOURNAL OF THE EARTH SCIENCES
Published by AGU and the Geochemical Society

Article
Volume 9, Number 9
30 September 2008
Q09006, doi:10.1029/2008GC002085
ISSN: 1525-2027

Upper crustal evolution across the Juan de Fuca ridge flanks

Mladen R. Nedimović
Department of Earth Sciences, Life Sciences Centre, Dalhousie University, Halifax, Nova Scotia B3H 4J1, Canada (mladen@dal.ca)

Lamont-Doherty Earth Observatory, Columbia University, Palisades, New York 10964, USA

Suzanne M. Carbotte and John B. Diebold
Lamont-Doherty Earth Observatory, Columbia University, Palisades, New York 10964, USA

Alistair J. Harding
Scripps Institution of Oceanography, University of California, San Diego, La Jolla, California 92093, USA

J. Pablo Canales
Woods Hole Oceanographic Institution, Woods Hole, Massachusetts 02543, USA

Graham M. Kent
Scripps Institution of Oceanography, University of California, San Diego, La Jolla, California 92093, USA

[1] Recent *P* wave velocity compilations of the oceanic crust indicate that the velocity of the uppermost layer 2A doubles or reaches ~4.3 km/s found in mature crust in <10 Ma after crustal formation. This velocity change is commonly attributed to precipitation of low-temperature alteration minerals within the extrusive rocks associated with ridge-flank hydrothermal circulation. Sediment blanketing, acting as a thermal insulator, has been proposed to further accelerate layer 2A evolution by enhancing mineral precipitation. We carried out 1-D traveltime modeling on common midpoint supergathers from our 2002 Juan de Fuca ridge multichannel seismic data to determine upper crustal structure at ~3 km intervals along 300 km long transects crossing the Endeavor, Northern Symmetric, and Cleft ridge segments. Our results show a regional correlation between upper crustal velocity and crustal age. The measured velocity increase with crustal age is not uniform across the investigated ridge flanks. For the ridge flanks blanketed with a sealing sedimentary cover, the velocity increase is double that observed on the sparsely and discontinuously sedimented flanks (~60% increase versus ~28%) over the same crustal age range of 5–9 Ma. Extrapolation of velocity-age gradients indicates that layer 2A velocity reaches 4.3 km/s by ~8 Ma on the sediment blanketed flanks compared to ~16 Ma on the flanks with thin and discontinuous sediment cover. The computed thickness gradients show that layer 2A does not thin and disappear in the Juan de Fuca region with increasing crustal age or sediment blanketing but persists as a relatively low seismic velocity layer capping the deeper oceanic crust. However, layer 2A on the fully sedimented ridge-flank sections is on average thinner than on the sparsely and discontinuously sedimented flanks (330 ± 80 versus 430 ± 80 m). The change in thickness occurs over a 10–20 km distance coincident with the onset of sediment burial. Our results also suggest that propagator wakes can have atypical layer 2A thickness and velocity. Impact of propagator wakes is evident in the chemical signature of the fluids sampled by ODP drill holes along the east Endeavor transect, providing further indication that these crustal discontinuities may be sites of localized fluid flow and alteration.

Copyright 2008 by the American Geophysical Union

Components: 13,053 words, 14 figures, 2 tables.

Keywords: upper crustal evolution; multichannel seismics; traveltime modeling; reflection imaging; Juan de Fuca ridge flanks.

Index Terms: 3035 Marine Geology and Geophysics: Midocean ridge processes; 3025 Marine Geology and Geophysics: Marine seismics (0935, 7294); 7220 Seismology: Oceanic crust.

Received 2 May 2008; **Revised** 20 June 2008; **Accepted** 29 July 2008; **Published** 30 September 2008.

Nedimović, M. R., S. M. Carbotte, J. B. Diebold, A. J. Harding, J. P. Canales, and G. M. Kent (2008), Upper crustal evolution across the Juan de Fuca ridge flanks, *Geochem. Geophys. Geosyst.*, *9*, Q09006, doi:10.1029/2008GC002085.

1. Introduction

[2] The Earth's oceanic crust crystallizes from magmatic systems generated at mid-ocean ridges. For ridges with fast to intermediate spreading rates, the lower section of the oceanic crust is composed of layered and massive gabbros on top of which lie diabase sheeted dykes and basaltic lavas of the upper oceanic crust. Tens of millions of years can pass until the oceanic crust formed at mid-ocean ridges is subducted, a time window providing much opportunity for crustal evolution to take place. Understanding how oceanic crust evolves is important from the perspectives of both basic science (e.g., energy and mass exchange between the Earth's solid interior and the oceans) and societal impacts (e.g., subduction earthquake hazards). Our knowledge about this evolutionary process remains limited because of the inaccessibility of the oceanic crust and the challenges associated with drilling and sampling it. For these reasons, geophysical surveying has played a major role in oceanic crustal studies during the past several decades.

[3] Early work on partitioning of the igneous oceanic crust into upper and lower seismic layers 2 and 3 [e.g., *Raitt*, 1963] was almost entirely based on interpretations of first arrival traveltimes. Researchers of the time noted that layer 2 velocities showed significant variation from location to location and speculated that much of this variation may originate within the top part of this layer. Based mostly on its magnetic properties, layer 2 was further subdivided into upper part A and lower part B [*Talwani et al.*, 1971]. This subdivision of layer 2 is still in use, and it is widely accepted that the steep vertical velocity gradient that defines the seismic layer 2A/2B boundary represents a porosity transition zone within the upper crust. However, the geologic nature of this porosity change continues to be debated, with two prevalent hypotheses: Layer 2A/2B boundary defines the geologic boundary between highly porous basaltic lavas and low-porosity diabase dykes [e.g., *Herron*, 1982; *Harding et al.*, 1993]; layer 2A/2B boundary is an alteration front in the upper crust, probably within the extrusive section [e.g., *Vera et al.*, 1990; *Christeson et al.*, 2007]. These two hypotheses may not be mutually exclusive for all mid-ocean ridges. For regions with a steady state magma chamber, with little or no off-axis variation in layer 2A thickness over time (e.g., East Pacific Rise), the well-defined base of layer 2A is likely both a lithologic boundary and alteration/permeability front.

[4] The first to make the correlation between the change in upper crustal seismic velocities and crustal evolution were *Houtz and Ewing* [1976] based on an analysis of sonobouy data from the North Atlantic and Pacific. They concluded that layer 2A velocities increase from 2.8 to 3.3 km/s at the ridge crests to >4.0 km/s on ridge flanks at about 40 Ma-old crust, and speculated that layer 2A likely changes with the passage of time through infilling of voids and cracks due to hydrothermal mineralization.

[5] Many approaches to investigating layer 2A velocity have been applied since the study of *Houtz and Ewing* [1976]. Most of these studies have extracted upper crustal velocity information from multichannel seismic (MCS) streamer data via 1-D modeling and inversion techniques such as interactive traveltime modeling [e.g., *Vera and Diebold*, 1994; *Rohr*, 1994], genetic algorithms [e.g., *Hussenoeder et al.*, 2002], or waveform inversion [e.g., *Collier and Singh*, 1998]. Other traveltime modeling studies were based on ocean bottom seismometer or expanding spread profile data [e.g., *Vera et al.*, 1990; *Christeson et al.*, 1993; *Grevemeyer et al.*, 1999]. The primary outcome of

these seismic studies is twofold: (1) *P* wave velocities within the layer 2A approximately double as it matures with increasing distance away from the ridge axis, which is the best documented change in the seismic structure of oceanic crust with age [*Purdy and Ewing*, 1986]; (2) Layer 2A thickness (100–200 m) at fast spreading ridges doubles or triples within a few km of the ridge axis [e.g., *Kent et al.*, 1994; *Carbotte et al.*, 2000], while intermediate to slow spreading ridges are typified by a thicker layer 2A section at the ridge crest, exhibiting modest changes in thickness near axis [e.g., *Blacic et al.*, 2004; *Canales et al.*, 2005]. These patterns of near-axis thickening may reflect differences in the accumulation of lavas linked to eruption parameters and ridge crest topography. Following the lead of *Houtz and Ewing* [1976], the velocity change within layer 2A has been commonly attributed to precipitation of low-temperature alteration minerals within the extrusive rocks associated with ridge flank hydrothermal circulation [*Jacobson*, 1992].

[6] Recent *P* wave velocity compilations indicate that at a regional scale layer 2A doubles in velocity within $\sim$ <10 Ma of crustal formation [*Grevemeyer and Weigel*, 1996; *Carlson*, 1998], much more quickly than originally interpreted by *Houtz and Ewing* [1976]. This increase in seismic velocity of layer 2A may not be a linear function of age. A multistage evolution is suggested by studies on the flanks of the fast spreading East Pacific Rise [*Grevemeyer and Weigel*, 1997] with rapid velocity increase at young ages (<1 Ma), a more gradual increase up to 5 Ma, gentle increase up to $\sim$10 Ma, and no change at greater age. *Grevemeyer and Weigel* [1997] attribute the variable layer 2A horizontal velocity gradient, horizontal rate of change in layer 2A velocity with respect to ridge-normal distance away from the spreading axis, to different rates of crustal alteration associated with ridge axis and flank hydrothermalism. Numerical simulations [*Fisher and Becker*, 1995; *Wang et al.*, 1997] and observational studies [e.g., *Langseth et al.*, 1988; *Johnson et al.*, 1993] point to a close relationship between hydrothermal upflow zones and basement relief further suggesting locally variable, topography driven mineral precipitation within layer 2A, and therefore locally variable 2A velocity increase.

[7] Sediment blanketing, acting as a thermal insulator, has been proposed by *Rohr* [1994] to enhance mineral precipitation within layer 2A and therefore accelerate the velocity increase with crustal aging. From analysis of a single MCS profile crossing the eastern Endeavor flank of the Juan de Fuca ridge, *Rohr* [1994] found an abrupt increase in layer 2A velocity at very young crustal ages (0.6–1.2 Ma) coincident with a transition from sediment-free to fully sediment-buried oceanic crust.

[8] Here we describe a systematic and uniform approach to extracting upper crustal *P* wave velocity and layer 2A thickness along hundreds of kilometers of long-streamer MCS profiles focused on gathering new information on oceanic crustal evolution. The primary motivation for this study was to examine on a regional scale the role of basement age and sediment burial on crustal alteration due to ridge flank hydrothermal circulation. We carried out 1-D traveltime modeling of upper crustal structure along ridge-normal MCS transects crossing the Endeavor, Northern Symmetric, and Cleft segments of the Juan de Fuca ridge. Data from a long hydrophone streamer are used to form a dense grid of analysis points, common midpoint (CMP) supergathers, spaced about every 3 km and extending across transects about 300 km long. This detailed approach to extracting upper crustal structure across the ridge axis, extending about 150 km away from the axis on both ridge flanks to 5–9 Ma-old crust, allows us to investigate both regional and local aspects of layer 2A evolution. The layer 2A velocity and thickness study presented in this paper is supported by coincident seismic reflection images, which were formed first to help guide the traveltime modeling. Along the Endeavor transect, which was positioned to coincide with the ODP/IODP Flank Flux experiment [*Davis et al.*, 1992, 1997], drill hole data provide direct constraints on crustal alteration and basement hydrogeologic conditions that can be used for correlation with the upper crustal seismic properties.

2. Study Area and Seismic Data

[9] The Juan de Fuca ridge, located offshore western North America (Figure 1), is the boundary between the Pacific and Juan de Fuca plates. This 480 km long, NNE-oriented intermediate-rate spreading center (56 mm/a full spreading rate [e.g., *Wilson*, 1993]) comprises seven 50–100 km long segments, each with a distinct axial morphology and separated by nontransform offsets up to 30 km in length. The Blanco and Sovanco fracture zones bound the Juan de Fuca ridge to the south and north, respectively. Several hundred kilometers to the east is the Cascadia subduction zone.

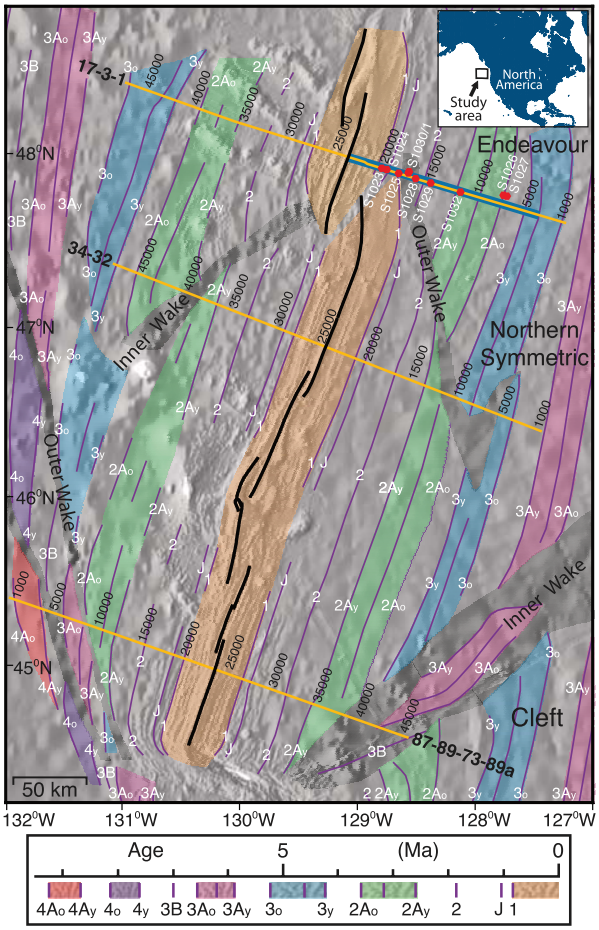

Figure 1. The 2002 Juan de Fuca ridge flank seismic profiles are plotted in orange over a Sun-illuminated gray bathymetric map. Every 5000th common midpoint (CMP) is annotated along each profile. Thick blue line underlining a part of the Endeavor transect shows the location of earlier seismic and heat-flow studies. Red hexagons are drill hole locations. Thick black lines are the interpreted traces of the ridge axis. Thin purple lines are magnetic isochrones [*Wilson*, 1988]. Their age is shown in the legend. Colored overlays outline areas of the crust formed during the normal magnetic periods. Gray overlay outlines the location of propagator wakes. The inset shows the location of the study area with respect to North America.

[10] The western and eastern Juan de Fuca ridge flanks are both crossed by propagator wakes but otherwise show prominent differences. Seamounts are found primarily on the Pacific plate, both as isolated edifices and in chains, several of which lie close to and intersect the Juan de Fuca ridge axis [*Davis and Karsten*, 1986]. Sediments covering the eastern Juan de Fuca ridge flank are up to a few kilometers thick at the northern Cascadia subduction deformation front [e.g., *Nedimović et al.*, 2003], and thin toward the ridge axis and southward away from the dominant source of terrigenous sediment. The western Juan de Fuca ridge flank is only sparsely sedimented, although sediment cover generally increases to the north.

[11] In 2002, we carried out an extensive MCS survey of the Juan de Fuca ridge and its flanks during R/V *Maurice Ewing* expedition EW0207. The MCS data were collected using a 6 km long, 480 channel Syntron digital towed hydrophone array, or streamer, with receiver groups spaced at 12.5 m. Streamer depth and feathering were monitored with a mix of 13 depth-controlling and 11 compass-enhanced DigiCourse birds, plus a GPS receiver on the tail buoy. A 10-element, 49.2 L (3005 in^3) tuned air gun array was used as the source of acoustic energy, with shots fired at a 37.5 m spacing under GPS control. Postshot listening time was 10.24 s and the returning acoustic energy was sampled at a 2 ms rate. Data were recorded on 3490E tapes in SEGD format using the Syntron Syntrack 480 seismic data acquisition system. The recorded signal has a bandwidth ranging from ~2 Hz to over 100 Hz. The nominal CMP bin spacing is 6.25 m and the nominal data trace fold is 80.

[12] Data were collected within the near axis region [*Canales et al.*, 2005, 2006; *Carbotte et al.*, 2006; *Van Ark et al.*, 2007] as well as along three ridge flank transects crossing the Cleft, Northern Symmetric and Endeavor segments and extending to crustal ages of 5–9 Ma [*Nedimović et al.*, 2005; *Carbotte et al.*, 2008] (Figure 1). Cleft, the southernmost segment crossed by the long transects, has a shallow and broad axial high notched by a 2–3 km wide axial rift flooded with recent lavas. Northern Symmetric (or Cobb) segment has a narrow, 1–2 km wide depression bisecting the crest of a narrow and deeper axial high. At Endeavor, the northernmost segment crossed by our long transects, abundant faulting is observed in the floor of a 2–3 km wide axial trough and there is little evidence for recent eruptions.

3. Data Analysis

3.1. Seismic Imaging

[13] The prestack processing strategy adopted for the EW0207 MCS data consisted of standard straight-line CMP bin geometry; F-K and bandpass (2-7-100-125 Hz) filtering to remove low-frequency towing noise; amplitude correction for geometrical

spreading; surface-consistent minimum phase predictive deconvolution to balance the spectrum and remove short period multiples; surface-consistent amplitude correction to balance anomalous shot and receiver-group amplitudes not related to wave propagation; trace editing; velocity analysis using the velocity spectrum method; normal moveout (NMO) and dip moveout (DMO) corrections to align signal for stacking; and CMP mute to remove overly stretched data. The prepared prestack data, with and without automatic gain control, were then stacked (averaged). The poststack processing included seafloor mute, primary multiple mute to reduce migration noise, trapezoidal bandpass filtering (2–7–100–125 Hz), and time migration to collapse diffractions and reposition dipping reflection events. To improve imaging within the oceanic plate below layer 2A/2B boundary, the late traveltime data were additionally bandpass filtered at 2–7–20–40 Hz and mildly coherency filtered.

[14] Extracting an image of the layer 2A/2B boundary, often referred to as the 2A event, requires a somewhat different processing scheme because this event is not a true reflection [*Harding et al.*, 1993]. The prestack data preparation is identical up to the velocity analysis, which is done on bandpass filtered (2-7-40-60 Hz) constant velocity stacks. When the normal moveout velocities that best flatten the retrograde branch of the 2A refraction are chosen, the data are subsequently stacked. The stacked layer 2A event is time migrated and coherency filtered. A surgical mute, used to zero unwanted parts of seismic data, is then applied to extract only the layer 2A event. Merging the extracted layer 2A event with the reflection section forms the final, composite seismic image.

[15] An example of a composite seismic image, transect 17–3–1 (see Figure 1 for location), is shown in Figure 2a. Reflections from the seafloor, sediment interfaces, top of the igneous basement, top of the axial magma chamber, and layer 2A/2B boundary event can all be identified. An enlarged section from the eastern part of this transect is shown in Figure 2b to emphasize the high quality of the collected data. Moho reflections, not shown in Figure 2, are also well imaged along all transects and are the focus of previous studies [*Nedimović et al.*, 2005; *Carbotte et al.*, 2008].

3.2. Traveltime Modeling

[16] We constructed about 6000 constant offset stack CMP supergathers as potential input for traveltime modeling of seismic arrivals. Each of the CMP supergathers is formed by combining data traces from 12 adjacent CMPs and then by stacking the traces with identical nominal source-receiver offsets. Some 300 of the CMP supergathers best suited for the analysis were then used for traveltime modeling in 1-D.

[17] Because the field data are characterized by 37.5 m shot spacing and 12.5 m receiver spacing, and the chosen CMP spacing is 6.25 m, the formed CMP supergathers have 480 data traces with stack fold of 2. We experimented with various CMP supergather configurations, starting from combining 6 adjacent CMPs and ending with combining 24 with an increment of 6, thus forming supergathers with 480 data traces and varying stack fold from 1 to 4. In most cases, the highest signal-to-noise ratio for the seismic arrivals of interest was achieved when combining 12 adjacent CMP gathers. This indicates that for our profiles, the lateral variations in two-way traveltime to igneous basement for traces with identical source-receiver offset become large enough to negatively affect the signal-to-noise ratio when stacking CMPs that are more than ~75 m apart.

[18] Our prestack data preparation for traveltime modeling of seismic arrivals is identical to that for the reflection imaging up to the NMO removal. CMP gathers without NMO correction are stacked into CMP supergathers and linearly moved out using velocity of 5500 m/s, the approximate velocity of the layer 2B refractions (Figures 3–5). CMP supergathers are then read into the JDseis software, which allows us to model reflection and refraction traveltime arrivals for constant velocity and linear velocity gradient layers (see Appendix A for a detailed description of JDseis software).

[19] Selecting and analyzing 300 CMP supergathers spaced at about every 3 km was a significant effort that resulted in a dense grid of 1-D upper crustal velocity functions and layer 2A thicknesses. The selected 300 CMP supergathers are located over the smoothest sections of the igneous basement and have the highest signal-to-noise ratio. These gathers are characterized by prominent seismic arrivals of interest, including triplications caused by the high vertical velocity gradient in the lower part of layer 2A. This is important for our study because observations of prominent layer 2A arrivals are not common; these waves are obscured by other stronger arrivals such as reflections and diffractions. The CMP geometry also greatly reduces possible effects of interface dip on the velocity analysis [*Diebold and Stoffa*, 1981].

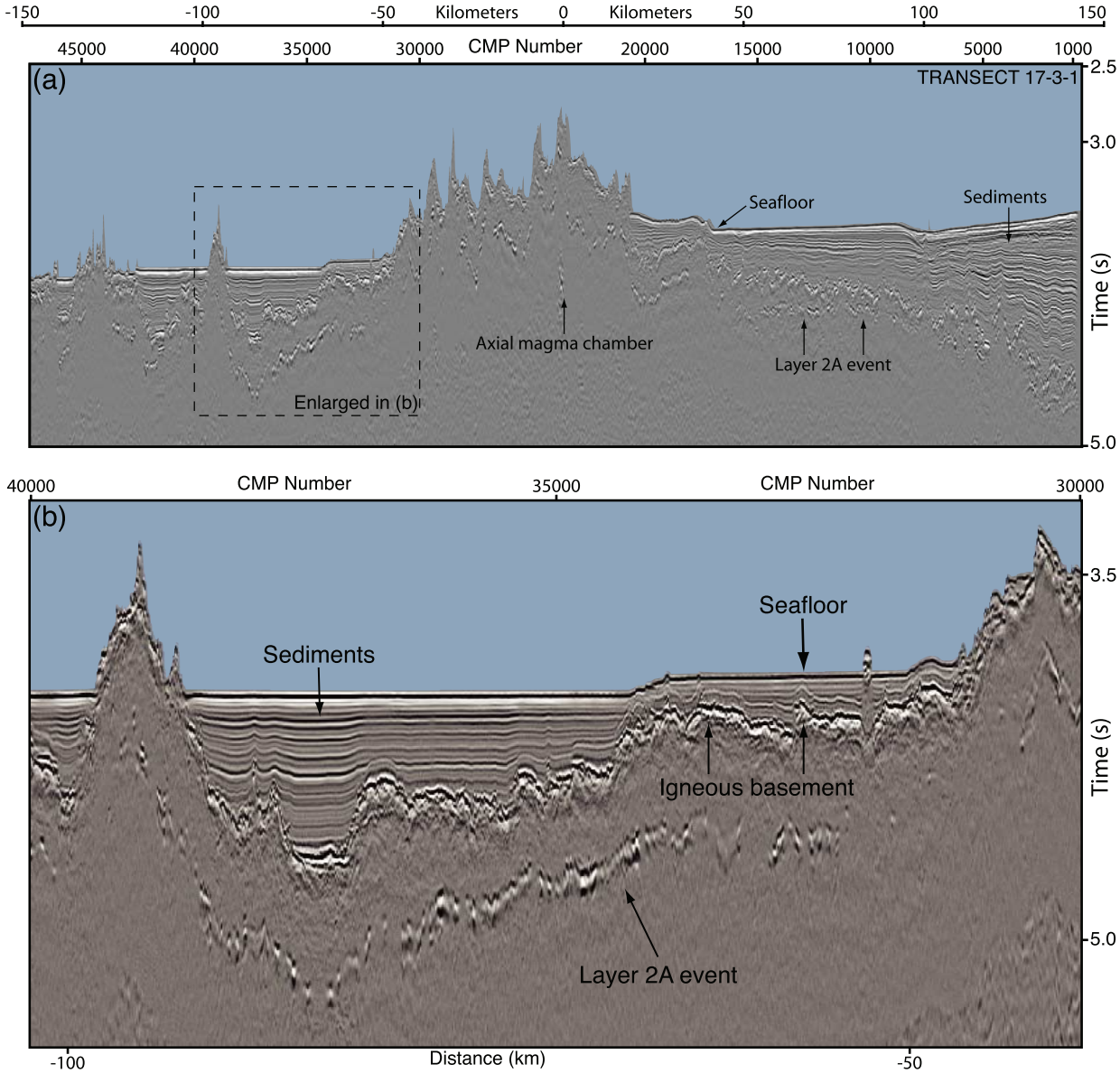

Figure 2. Seismic reflection image of the Endeavor transect 17–3–1 formed by analyzing MCS data collected during the 2002 EW0207 cruise. (a) Sediments, crystalline basement, layer 2A/2B boundary and axial magma chamber are generally all well imaged. (b) Strength of the layer 2A/2B boundary "reflection" can better be visualized. Figure 2b is an enlarged image of the area outlined by the dashed box in Figure 2a. Where imaged, the 2A/2B seismic event varies in strength from strong to weak.

[20] Three example CMP supergathers from each of the investigated long transects crossing Endeavor, Northern Symmetric, and Cleft ridge segments, with and without modeled seismic traveltime arrivals, are shown in Figures 3, 4, and 5, respectively. Also shown are velocity models used to compute the seismic traveltime arrivals. For all transects investigated, the three CMP supergathers presented cover a range of geologic environments, from the heavily sedimented eastern ridge flank, to the thinly sedimented or sediment-barren igneous crust on the western ridge flank or near the ridge axis. The traveltime modeling on CMP supergathers was carried out by assuming a four or five layer model, depending on the presence or absence of sediments at the investigated location. Seawater and sediment column were modeled as constant velocity layers. Upper layer 2A, lower layer 2A, and uppermost

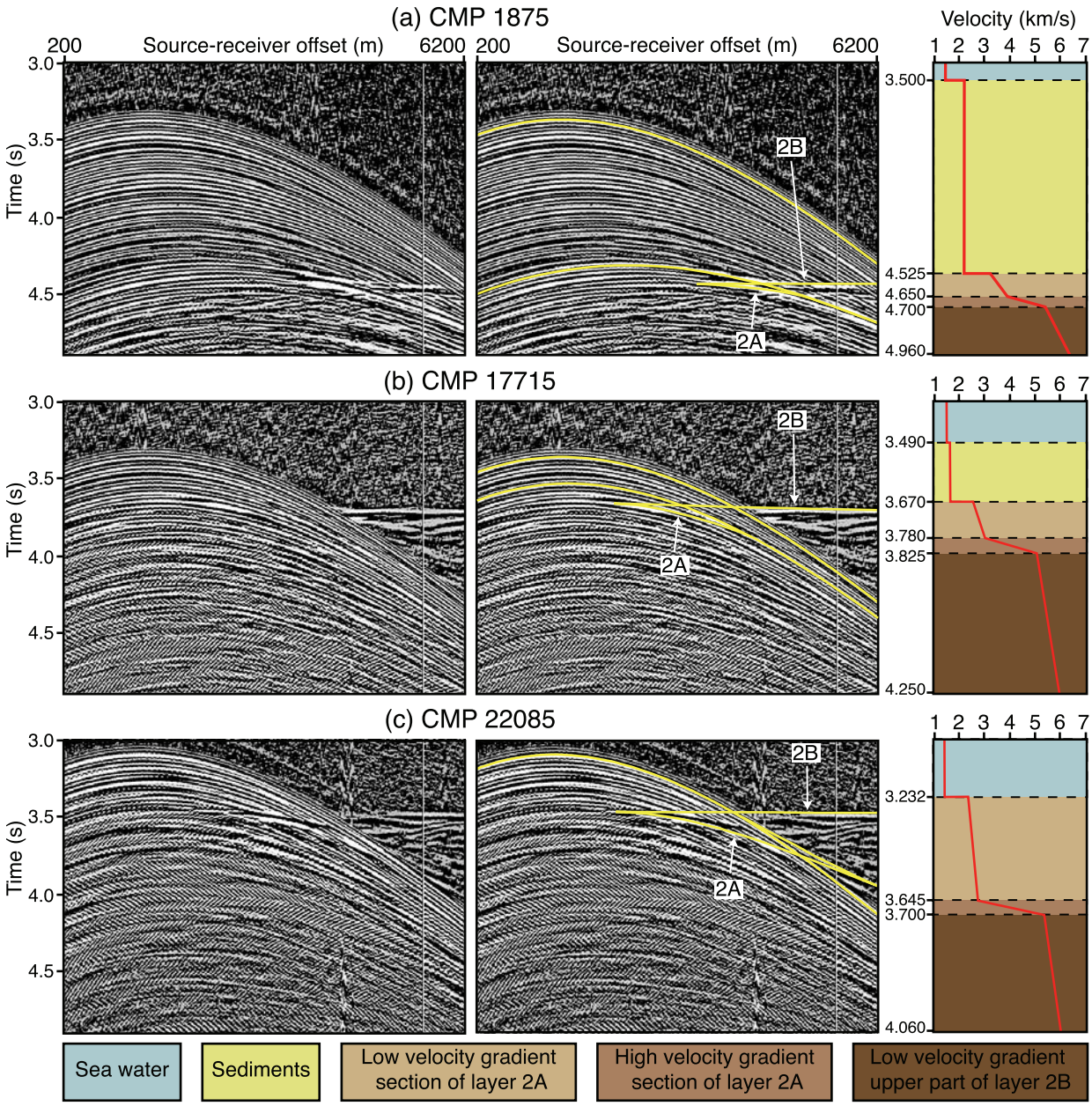

Figure 3. Traveltime curves and the resulting model velocities for selected CMP supergathers (a) 1875, (b) 17,715, and (c) 22,085 from the Endeavor transect 17–3–1. The left images show the CMP supergathers corrected using a linear moveout (LMO) with velocity of 5500 m/s. Middle images show the same information as the corresponding images in the left column but also include modeled traveltime arrivals (yellow lines) for the seafloor reflection, igneous basement reflection, layer 2A refraction (turning ray), and layer 2B refraction. Right images show the velocity models that correspond to the fitted traveltime curves shown in the middle column images.

layer 2B were modeled as linear-vertical-gradient velocity layers.

4. Results

[21] Seismic imaging and traveltime modeling results for the three long transects crossing Endeavor, Northern Symmetric, and Cleft ridge segments are summarized in Figures 6 and 7. In Figure 6, the relationship between the imaged upper crustal structure and layer 2A velocities is compared. Figure 7 shows the relationship between the imaged upper crustal structure and layer 2A thickness. The upper crustal structure in both Figures 6

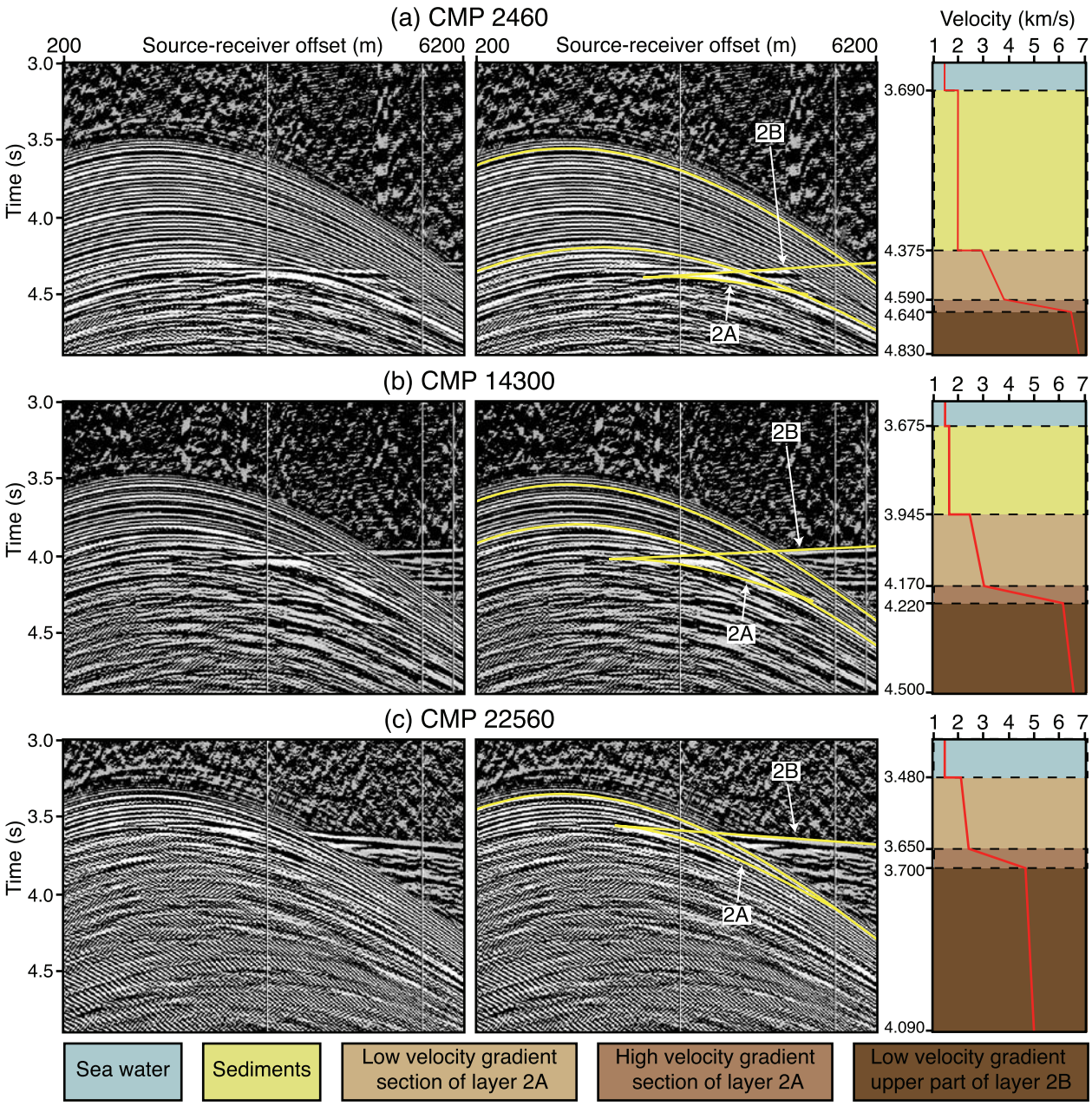

Figure 4. Traveltime curves and the resulting model velocities for selected CMP supergathers (a) 2460, (b) 14,300, and (c) 22,560 from the Northern Symmetric transect 34–32. Left images show the CMP supergathers corrected using an LMO and velocity of 5500 m/s. Middle images show the same information as the corresponding images in the left column but also include modeled traveltime arrivals (yellow lines) for the seafloor reflection, igneous basement reflection, layer 2A refraction (turning ray), and layer 2B refraction. Right images show the velocity models that correspond to the fitted traveltime curves shown in the middle column images.

and 7 (top) is presented by traveltime picks of seismic arrivals most important for this study, those coming from the seafloor, top of the igneous basement, layer 2A/2B boundary, and top of the axial magma chamber. Seafloor and igneous basement are imaged continuously. The layer 2A/2B pseudo reflection event is imaged along much of each transect. Average upper layer 2A velocities and average whole layer 2A velocities (Figure 6, middle and bottom), as well as upper layer 2A thicknesses and whole layer 2A thicknesses (Figure 7, middle and bottom) are all presented in the context of distance from the ridge axis, crustal age, sediment cover, and propagator wake distribution.

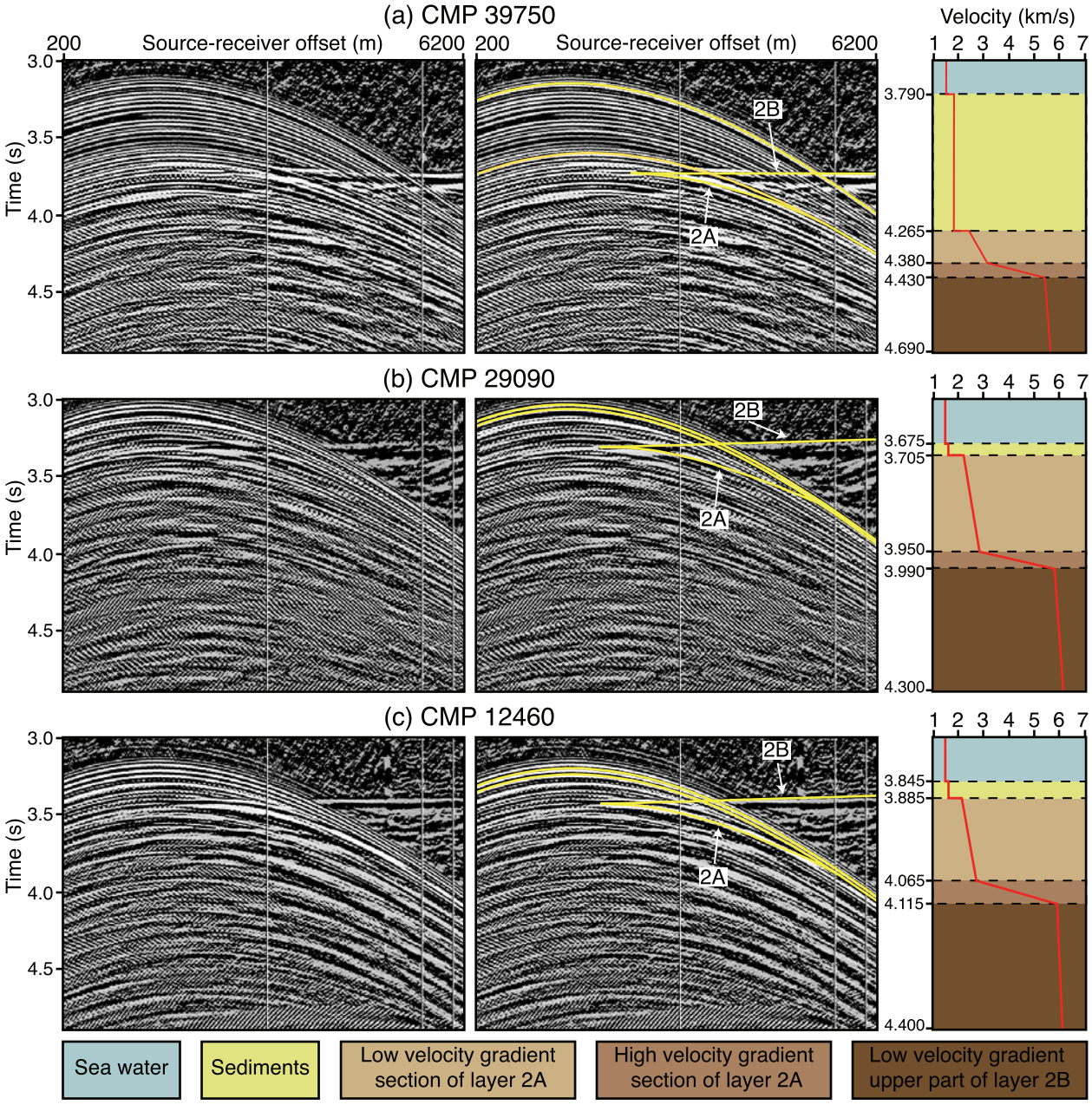

Figure 5. Traveltime curves and the resulting model velocities for selected CMP supergathers (a) 39,750, (b) 29,090, and (c) 12,460 from the Cleft 87–89–73–89a transect. Left images show the CMP supergathers corrected using an LMO and velocity of 5500 m/s. Middle images show the same information as the corresponding images in the left column but also include modeled traveltime arrivals (yellow lines) for the seafloor reflection, igneous basement reflection, layer 2A refraction (turning ray), and layer 2B refraction. Right images show the velocity models that correspond to the fitted traveltime curves shown in the middle column images.

[22] Uncertainties for measurements of seismic layer velocity and thickness presented in Figures 6 and 7 vary at each CMP supergather location depending on many parameters such as data signal-to-noise ratio, range of offsets over which seismic arrivals can be identified, smoothness and dip of the layer boundaries, and sediment thickness. We carried out a sensitivity analysis to determine the range of permissible model parameters that fit the data. From the maximum and minimum fits, we estimated average uncertainties in individual CMP supergather measurements of velocity and thickness to be: Upper layer 2A average velocity, ±150 m/s; lower layer 2A average

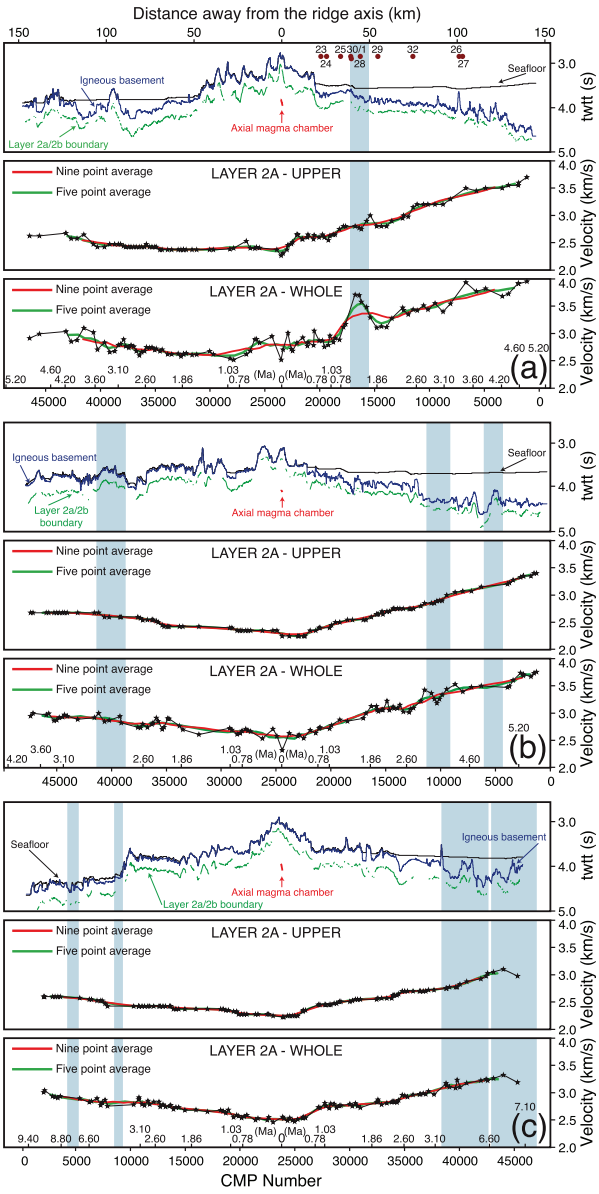

Figure 6. Crustal seismic structure and layer 2A velocity results for the (a) Endeavor (17–3–1), (b) Northern Symmetric (34–32), and (c) Cleft (87–89–73–89a) MCS transects. Top sections show seismic structure. Middle and lower parts show 2A velocity results. Black stars connected with a thin black line are average upper 2A and whole 2A velocities from 1-D traveltime velocity analysis on CMP supergathers. Shaded areas outline the location of propagator wakes. Brown circles in Figure 6a are drill hole locations. All drill holes are missing 10 in front of the number (e.g., 23 is drill hole 1023). CMP number, crustal age, and distance from the ridge axis are all given on the horizontal axis.

velocity, ±120 m/s; uppermost layer 2B average velocity, ±100 m/s; upper layer 2A thickness, ±30 m; lower layer 2A thickness, ±10 m.

4.1. Seismic Images

[23] Reflection sections (Figures 2, 6, and 7) show that the western and eastern Juan de Fuca ridge flanks are evolving in a markedly different way due to distinct sedimentary and volcanic histories. Hemipelagic sediments that thin southward are much thicker and more extensive on the eastern ridge flank. Enhanced accumulation of sediment on the eastern flank is in large part caused by the

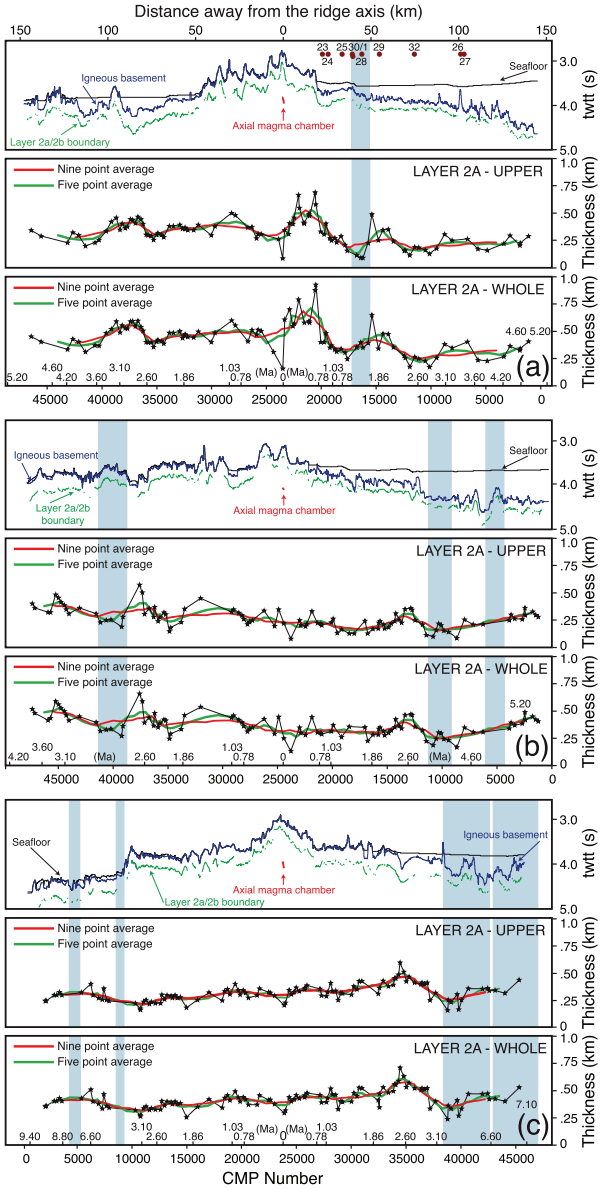

Figure 7. Crustal seismic structure and layer 2A thickness results for the (a) Endeavor (17–3–1), (b) Northern Symmetric (34–32), and (c) Cleft (87–89–73–89a) transects. Top sections show seismic structure. Middle and lower parts show 2A thickness. All the annotation in Figure 7 is identical to the annotation presented in Figure 6.

Table 1. Computed Average Upper, Lower, and Whole Layer 2A Thicknesses for the Investigated Juan de Fuca Ridge Flanks

Ridge Flank	Average Layer 2A Thickness[a]		
	Upper	Lower	Whole
East Endeavor	220 ± 70	100 ± 30	320 ± 80
East North Symmetric	220 ± 70	110 ± 30	330 ± 80
East Cleft	350 ± 90	110 ± 10	460 ± 90
West Endeavor	350 ± 70	110 ± 20	460 ± 80
West North Symmetric	340 ± 80	100 ± 10	440 ± 90
West Cleft	270 ± 50	110 ± 10	380 ± 50

[a] Average layer 2A thickness is measured in meters.

morphology of the Juan de Fuca ridge, with its cooling and subsiding flanks forming basin-like depositional environments and its elevated axial region acting as a barrier that inhibits the transport of terrigenous sediment to the western flank.

[24] Sediments across the north-central section of the eastern ridge flank completely cover the igneous basement starting 20–30 km east from the ridge axis (Figures 6a and 6b, top). However, this thermal blanketing of igneous basement [e.g., *Wheat and Mottl*, 1994] does not appear to be present in the southern section (Figure 6c, top) because the sedimentary cover in the area is pierced by many basement highs that may act as basement ventilators. Sedimentary cover on the western flank is generally thin and discontinuous due to the abundance of seamount volcanism [*Davis and Karsten*, 1986], although some isolated pockets of thicker accumulations are identified in the north.

4.2. Layer 2A Velocities and Thicknesses

[25] Layer 2A velocities (Figure 6) show a systematic increase with distance from the ridge axis that differs in magnitude between the seismic transects and within each transect across the eastern and western ridge flanks. On the eastern flank, there is a significant increase in layer 2A velocities of about 60% along the Endeavor (~2.5–4.0 km/s) and Northern Symmetric (~2.3–3.7 km/s) transects as the crust ages from 0 to 5–7 Ma. East of the Cleft ridge segment, along the southern transect, the velocity increase is smaller (approximately 32%; ~2.5–3.3 km/s). Similar to the east Cleft transect, more modest increase in layer 2A velocity with crustal age is identified across the western ridge flank. For west Endeavor, Northern Symmetric, and Cleft transects the velocity increases are about 24% (~2.5–3.1 km/s), 30% (~2.3–3.0 km/s), and 24% (~2.5–3.1 km/s), over approximately 5, 4, and 9 Ma, respectively.

[26] There are no systematic variations in layer 2A thickness with distance from the ridge axis along any of the transects (Figure 7). However, average layer 2A thicknesses along the eastern Endeavor and eastern Northern Symmetric flanks are less than that along the eastern Cleft and all of the western flanks (see Table 1). Similar transect-to-transect differences in average thicknesses are observed for the low velocity gradient upper section of layer 2A but not for the high-velocity gradient lower section of layer 2A, whose thickness shows less variation (Table 1). Therefore, much of the variability in layer 2A thickness measured from one ridge segment to another originates within the low-velocity gradient upper section of layer 2A. Thickness estimates for very young crust (<1 Ma), where constructional volcanism may still be taking place, were excluded from the computation of average thicknesses shown in Table 1.

[27] The traveltime modeling results accurately reveal regional layer 2A velocity increases and 2A thickness changes. Variability of layer 2A velocity and thickness, from one 1-D analysis to another, diminishes from north (Endeavor transect) to south (Cleft segment). Shorter wavelength variations in layer 2A velocity and thickness, superimposed on the long-term systematic trends, are also apparent. Nevertheless, because of the still limited lateral resolution of our dense 1-D study, we restrict our discussion to velocity and thickness anomalies that laterally extend for more than 5–10 km.

5. Discussion

[28] The results presented in this work are compared to observations of layer 2A evolution evident in existing global syntheses of *Carlson* [1998] and *Grevemeyer et al.* [1999]. Regionally, we compare our east Endeavor segment results with those from the coincident study of *Rohr* [1994] and the results of ODP/IODP Flank Flux experiment [*Davis et al.*, 1992]. Additional constraints on the oceanic crustal structure on the flanks of the Juan de Fuca ridge are available from a number of refraction and other reflection studies conducted since the 1980s. However, results from these studies (e.g., *Cudrak and Clowes* [1993], *Barclay and Wilcock* [2004], *McClymont and Clowes* [2005], and *Van Ark et al.* [2007] for Endeavor; *McClain and Lewis*

Table 2. Computed Layer 2A *P* Wave Velocity and Thickness Gradients for the Investigated Juan de Fuca Ridge Flanks[a]

Ridge Segment	Eastern Flank	Western Flank
	Layer 2A Thickness Gradient	
Endeavor	−13 ± 14	−19 ± 13
Northern Symmetric	15 ± 9	29 ± 25
Cleft	−8 ± 8	5 ± 3
	Layer 2A P Wave Velocity Gradient	
Endeavor	0.271 ± 0.013	0.103 ± 0.011
Northern Symmetric	0.213 ± 0.008	0.117 ± 0.011
Cleft	0.120 ± 0.005	0.109 ± 0.007

[a]Layer 2A thickness gradient is measured in m/Ma and layer 2A *P* wave velocity gradient is measured in km s^{-1}/Ma.

[1982] and *Christeson et al.* [1993] for Northern Symmetric; and *McDonald et al.* [1994] and *Canales et al.* [2005] for Cleft) are not suitable for a systematic regional-scale comparison with the results extracted here as they either have limited resolution within the shallowest crust or are too widely spaced even when combined.

5.1. Impact of Crustal Age

5.1.1. Crustal Age and Layer 2A Velocity

[29] Average layer 2A *P* wave velocities across the Juan de Fuca ridge flanks systematically increase with distance from the ridge axis, or with crustal age, as observed on ridge flanks globally [e.g., *Carlson*, 1998; *Grevemeyer and Bartetzko*, 2004]. However, this velocity increase is not uniform. To quantify the rate of change of velocity with crustal age and test the hypothesis that layer 2A velocities double within 10 Ma [e.g., *Purdy*, 1987; *Rohr*, 1994; *Grevemeyer and Weigel*, 1996], we fit the velocity data from each ridge flank separately. Although the "eyeball" fit of the median velocities from *Carlson* [1998] global synthesis suggests a power law for the relationship between layer 2A velocity and crustal age, we choose simple linear regression (least square fit of a straight line) because it results in smaller residuals and appears most appropriate for our data set. During fitting we removed the data outliers due to anomalous crust in propagator wakes. Examples include the propagator wake along the eastern Endeavor ridge flank and the crust west of CMP 8000 on the Cleft transect, where crustal age cannot be determined accurately due to two closely spaced propagator wakes (Figures 1 and 6). Final regressions were done on ~95% of the original measurements. Computed horizontal velocity gradients for all investigated flanks are shown in Table 2.

[30] We use a linear extrapolation of the trends computed on ~0–6 Ma-old crust to estimate the crustal age at which the layer 2A velocity will be double that found on the ridge axis. Our results suggest that the layer 2A velocities across the eastern ridge flank for the Endeavor and Northern Symmetric transects double by an age of ~9 and ~11 Ma, respectively, compared with ~25, ~20, and ~23 Ma for the western Endeavor, Northern Symmetric, and Cleft ridge flanks. For the layer 2A velocities to double along the eastern Cleft ridge flank it is estimated that the crust has to age for ~21 Ma, significantly more than that along the eastern Endeavor and eastern Northern Symmetric ridge flanks, and more in line with the estimates for the western ridge flanks. If the layer 2A velocity increase is better described by a power law [*Carlson*, 2004] or by a smoothly varying polynomial [*Grevemeyer and Weigel*, 1996], as suggested for the global velocity data set, then doubling of layer 2A velocities along the Juan de Fuca ridge flanks would take longer than estimated here.

[31] Another approach to evaluating crustal evolution is to estimate crustal age at which layer 2A reaches velocities typical for mature oceanic crust [e.g., *Grevemeyer et al.*, 1999]. For the eastern flanks of the Endeavor, Northern Symmetric, and Cleft ridge segments we estimate using linear extrapolation that the velocity of ~4.3 km/s is reached at ~7, ~9, and ~15 Ma, respectively. For the western flanks, the corresponding ages are ~17, ~17, and ~16 Ma.

[32] Crustal ages computed by linear extrapolation of layer 2A velocities in both cases lead to similar conclusions. The results for the eastern Endeavor and eastern Northern Symmetric ridge flanks, which are blanketed with a sealing sedimentary cover, are consistent with the hypotheses that layer 2A velocities double or reach mature oceanic crust values of ~4.3 km/s within <10 Ma [*Grevemeyer et al.*, 1999; *Purdy*, 1987; *Grevemeyer and Weigel*, 1996]. The other four flanks, those with thin and discontinuous sediment cover, show a more gradual increase in layer 2A velocities, reaching ~4.3 km/s within 15–17 Ma.

[33] To further investigate the relationship between the Juan de Fuca ridge flank layer 2A velocities analyzed here and the existing global database [*Carlson*, 1998; *Grevemeyer et al.*, 1999] we plot the two together in Figure 8. Velocities from our

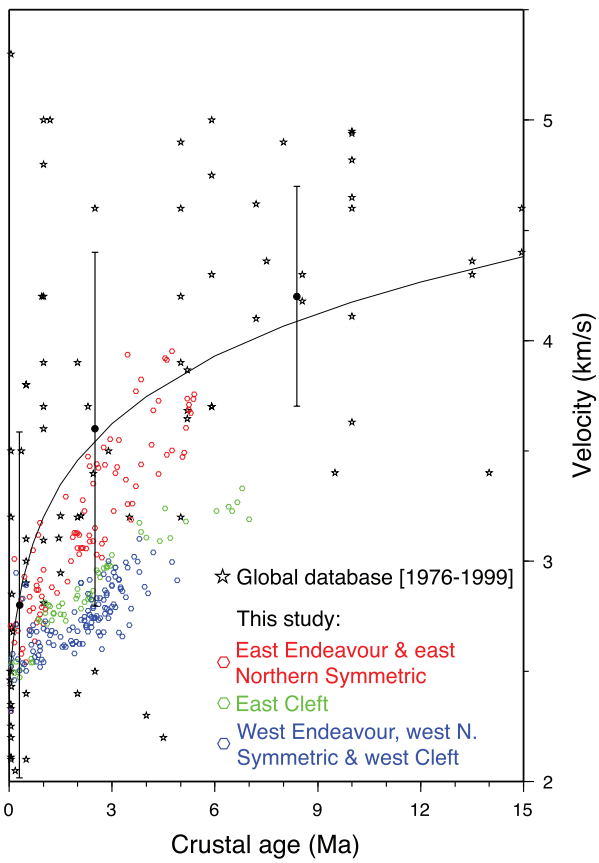

Figure 8. Average layer 2A *P* wave velocities as a function of crustal age for the first 15 Ma of crustal evolution. Stars are both velocities compiled by *Carlson* [1998] for years 1976 to 1997 and velocities from *Grevemeyer et al.* [1999] from an investigation designed to study upper crustal aging along the East Pacific Rise at 14°S. Solid black circles with error bars are mean velocities from *Carlson* [1998] for ages <1 Ma, ≥1 and ≤5 Ma, and >5 and <20 Ma. Thin black line is the power law fit of the global data set (stars) from *Carlson* [2004]. Hexagons are velocities from this study. Fully sedimented Endeavor and Northern Symmetric eastern flanks are shown in red; partially sedimented Cleft eastern flank is shown in green; barren or thinly and sparsely sedimented western flanks are shown in blue. Note that the velocity analysis done for this study was a significant effort that resulted in three to four times as many layer 2A velocity data points as there are in the global compilation [*Carlson*, 1998; *Grevemeyer et al.*, 1999], but that these velocities characterize a relatively small and unique region of the oceanic crust.

study show a similar trend of velocity increase with greater crustal age but are less scattered than the global database. Several factors may contribute to the lower scatter we observe. Unlike the global database, which includes studies of oceanic crust created at different spreading rates using a broad range of seismic data sets (mostly wide-angle) and applying different traveltime analysis techniques, the current study was of a relatively uniform intermediate-spread crust using a single MCS data set and a uniform traveltime analysis technique. The newly computed velocities also show a more gradual increase with crustal age than the prior compilations and do not seem to follow the power law function as suggested by the mean velocities computed here for the global compilation of *Carlson* [1998] and *Grevemeyer et al.* [1999].

5.1.2. Crustal Age and Layer 2A Thickness

[34] Many research projects have been directed toward investigating layer 2A [e.g., *Kennett and Orcutt*, 1976; *Whitmarsh*, 1978; *Stephen and Harding*, 1983; *McClain and Atallah*, 1985; *Minshull et al.*, 1991; *Christeson et al.*, 1994] since the seminal paper by *Houtz and Ewing* [1976]. Because these investigations were usually done over a relatively small section of the oceanic crust, they could not individually address one of the key hypotheses proposed by *Houtz and Ewing* [1976] that layer 2A "thins" with increasing crustal age and eventually becomes seismically indistinguishable from layer 2B. By the mid-1990s, however, there were enough observations from individual seismic refraction experiments to compile a database [*Grevemeyer and Weigel*, 1996], expand it to include drillhole results [*Carlson*, 1998], and statistically analyze it. From his analysis *Carlson* [1998] concludes that layer 2A does not disappear with increasing crustal age but persists as a region of relatively lower seismic velocities capping the oceanic crust.

[35] Statistical analysis done by *Carlson* [1998] cannot be applied to our data as most of our traveltime modeling was done on young oceanic crust (0–5 Ma) and at no place, even within the older crust (5–9 Ma), do the layer 2A velocities reach those found in the mature oceanic crust (~4.3 km/s). Therefore, to further contribute to the work of *Houtz and Ewing* [1976] and *Carlson* [1998], we take a direct approach and investigate the fate of layer 2A along the Juan de Fuca ridge flanks by fitting the layer 2A thickness data from each ridge flank both independently and jointly. Long-term thickness trends are calculated excluding results from young crust (0–1 Ma) that may be affected by accretionary processes at the ridge axis.

[36] The computed thickness gradients (see Table 2) for one half of the investigated flanks are negative (Endeavor east, Endeavor west, and Cleft east), and

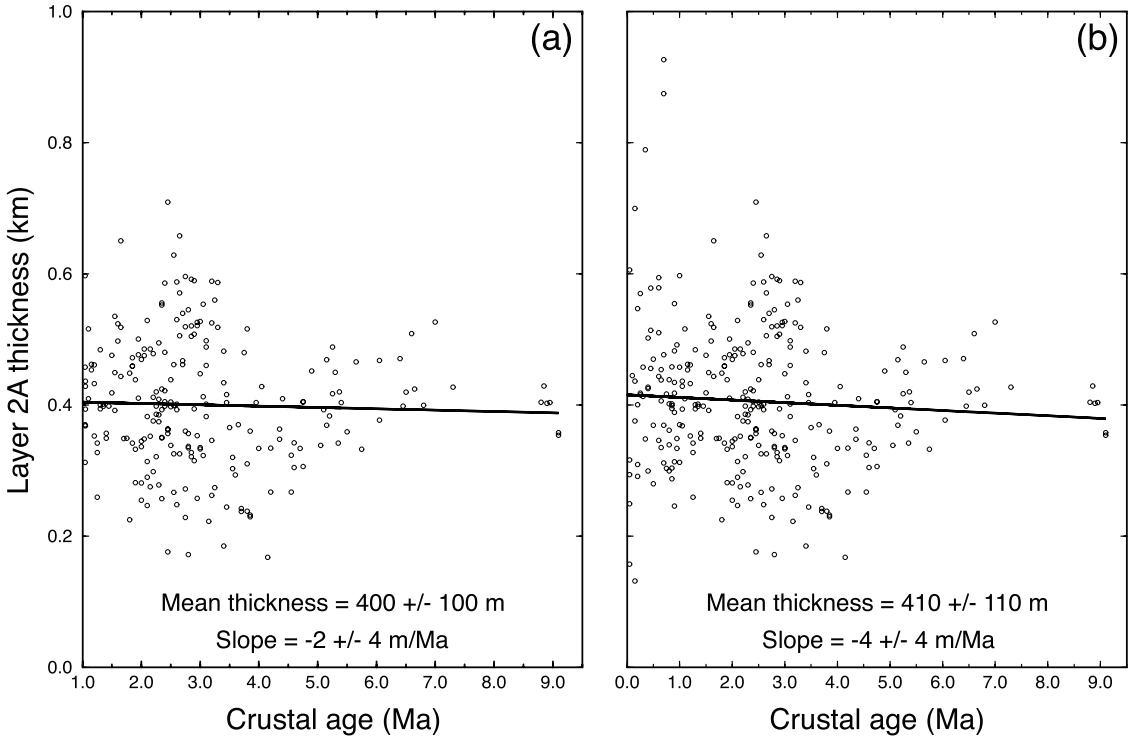

Figure 9. Layer 2A thickness in the Juan de Fuca region as a function of oceanic crustal age. (a) Mean thickness and thickness gradient for crustal ages 1 Ma and older. (b) Mean thickness and thickness gradient for the whole database, from 0 to ~9 Ma old crust.

for the other half are positive (Northern Symmetric east, Northern Symmetric west, and Cleft west). This points to lack of systematic variation of layer 2A thickness with increasing crustal age for the Juan de Fuca region. Furthermore, the errors in the computed thickness gradients (Table 2) are of about the same magnitude as the gradients themselves, so thinning of layer 2A with increasing crustal age is not statistically significant even for individual flank transects with negative thickness gradients.

[37] Figure 9a, where the relationship between layer 2A thickness and crustal age for all six transects is jointly examined, lends further support for the conclusion that the layer 2A is not gradually thinning and disappearing in the Juan de Fuca region. The computed thickness gradient of -2 ± 4 m/Ma indicates that there is no systematic change in layer 2A thickness of some 400 m (400 ± 100 m mean value) with changing crustal age throughout the region. In Figure 9b, we plot the same data set as in Figure 9a but include thickness values determined for the first 1 Ma of oceanic crust. Despite what appear to be several outliers in the young oceanic crust, regression values for the whole data set differ little from those computed for crust older than 1 Ma.

5.2. Impact of Sediment Cover

5.2.1. Sediment Cover and Layer 2A Velocity

[38] Sedimentary cover is believed to exert important control on the process of hydrothermal deposition within the upper igneous crust [e.g., *Jacobson*, 1992; *Alt*, 1995]. In particular when the sediments are sealed and are insulating layer 2A from the seawater above, the resulting higher basement temperatures hasten the alteration of basalts. At the Endeavor segment, basement temperatures increase from <10°C near the ridge axis, where there are no sediment deposits, to 40–50°C some 20 km east from the onset of the continuous sedimentary cover [*Davis et al.*, 1992; *Wheat and Mottl*, 1994]. For the low temperature alteration regime (<150°C) [*Hunter et al.*, 1999], a significant change such as this could speed up the hydrothermal deposition which could affect layer 2A velocity to a degree that can be detected using seismic techniques in addition to the crustal aging effect. This is possible because large changes in

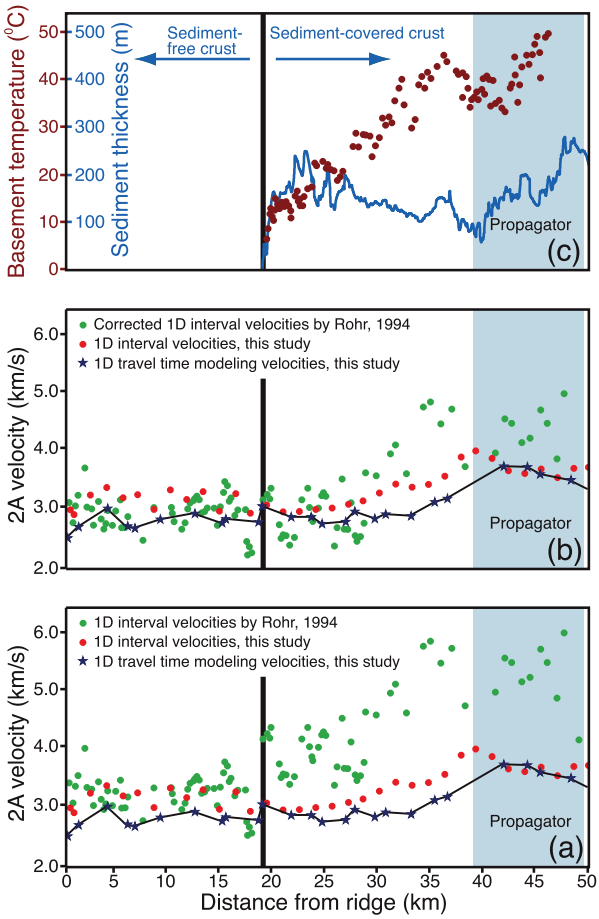

Figure 10. Comparison of layer 2A velocities from two coincident surveys over the Endeavor ridge segment. (a) Purple stars connected by a thin black line are new layer 2A velocities extracted by 1-D traveltime modeling on CMP supergathers from the 2002 MCS data set. Red dots are new layer 2A interval velocities extracted from analyzed stacking velocities. Green dots represent the same type of information as red dots but are based on an earlier study and data by *Rohr* [1994]. (b) Same as Figure 10a but with velocities represented by green dots corrected as suggested by *Rohr* [1994]. (c) Sediment thickness from this study and basement temperature results from the heat flow studies by *Davis et al.* [1997].

seismic velocity can be generated with small reduction in total porosity by preferential sealing of low aspect ratio (thin) cracks [*Wilkens et al.*, 1991].

[39] The differences in the increase of layer 2A velocity as a function of crustal age between individual ridge flanks (see section 5.1.1) are directly correlatable with the distribution and characteristics of the sedimentary cover within the Juan de Fuca region (Figure 6). The largest velocity increase with age is found in the north central part of the eastern Juan de Fuca ridge-flank region (east Endeavor and east Northern Symmetric flanks), where the most continuous and thickest sedimentary cover is imaged (Figure 8). In this area, there are only a few isolated basement outcrops [e.g., *Fisher et al.*, 2003]. The rate of change in layer 2A velocity as a function of crustal age decreases as the continuity and thickness of the sediments are reduced southward to the moderately sedimented east Cleft flank and to the sparsely sedimented igneous crust on the western ridge flanks.

[40] Comparison between the influence of the sediment thickness and continuity of sedimentary cover shows that the latter appears to have a greater effect on the layer 2A evolution. Sealing sedimentary cover appears to double the effect of crustal aging on layer 2A velocities, as evidenced at the east Endeavor and east Northern Symmetric ridge flanks. The east Cleft and west Endeavor flanks, where significant sediment accumulations are confined to minibasins between large basement outcrops, show similar horizontal gradients in layer 2A velocity as the west Northern Symmetric and west Cleft flanks, which are sparsely sedimented or sediment starved (Table 2).

5.2.2. Comparison With Earlier Results

[41] Overall, our results are consistent with the rapid increase in 2A velocities with sealing sediment cover at the east Endeavor ridge flank found in the earlier study of *Rohr* [1994]. However, despite general agreement in the velocity trend, there are important differences between the two investigations in the upper crustal velocities obtained. In Figure 10a the estimated layer 2A velocities from both studies are presented for the 50 km section east of the Endeavor ridge where the MCS profile analyzed by *Rohr* [1994] and the EW0207 transect 17–3–1 are coincident. Within the 19 km closest to the ridge axis, where there is no measurable sedimentary cover, average layer 2A velocities from this study (stars in Figure 10a) are lower than *Rohr*'s [1994] layer 2A interval velocities (green circles) by some 0.5 km/s, on average. This difference becomes much greater, on the order of ~2 km/s, for the sedimented section (19–50 km).

[42] Interval velocities for the *Rohr* [1994] study are estimated from stacking velocities using the *Dix* [1955] method that applies well to a horizontally stratified earth with constant velocity layers but not so well for layer 2A with its velocity gradients and velocity gradient reflections. On the

basis of comparisons between the Dix solutions and forward traveltime models for known velocity structure *Rohr* [1994] concludes that the Dix approximation has overestimated the interval velocity of layer 2A by ~0.3 km/s for the nonsedimented section, and by as much as 1 km/s for the sedimented section of the east Endeavor profile. We use this analysis to correct and replot velocities from *Rohr* [1994] for a better comparison of layer 2A velocities [Figure 10b]. We also compute layer 2A interval velocities for our study using the same approach as *Rohr* [1994] and plot them (red circles in Figures 10a and 10b) without the correction estimated by *Rohr* [1994].

[43] Figure 10b shows that the corrected *Rohr* [1994] velocities for the unsedimented section of the profile and for the first 10 km of the sedimented section mostly agree with velocities from this study, although they remain marginally higher in particular for the 15 km closest to the ridge axis. For the profile section from 30 to 50 km, corrected *Rohr* [1994] velocities remain significantly higher than the velocities from this study. At a greater distance from the ridge axis, from 50 to ~150 km along the profile (not shown in Figure 10), layer 2A velocities in *Rohr* [1994] maintain an average value of ~5.5 km/s (~4.5 km/s after correction), while velocities in this study only gradually increase to ~4 km/s.

[44] Interval velocities computed in this study from stacking velocities (Figures 10a and 10b) for comparison with the same from *Rohr* [1994] are for the most part higher than the average layer 2A velocities computed from the results of our traveltime modeling. The mean difference between the two estimates is ~0.35 km/s for the unsedimented and ~0.25 km/s for the sedimented section of the profile. Interestingly, this is in agreement with the *Rohr* [1994] estimate for the unsedimented crust (~0.3 km/s), but much less than was suggested for the sedimented crust (up to 1 km/s). As such, interval velocities from this study show improved agreement with the corrected interval velocities from *Rohr* [1994] (Figure 10b). However, even after applying the velocity corrections, the key features of the velocity mismatch persist.

[45] We attribute the disagreement in the estimated layer 2A velocities between the two studies to the traveltime analysis techniques applied and the different vintage data used. The most important difference between the two spatially coincident data sets is that ours was collected some 15 years later with about twice as long streamer and digital technology, providing longer source-receiver offset information and ensuring improved data quality. Having larger offsets turned out to be important for imaging and traveltime modeling as the layer 2A refraction for the Juan de Fuca region turns at distances between about 2 and 4.5 km (Figures 3, 4, and 5). Far offsets are particularly important for investigating the sedimented sections of the ridge flanks as the basement in this area becomes deeper and layer 2A refractions occur at the higher end of the 2 to 4.5 km offset range (Figures 3, 4, and 5).

[46] Data analysis for the *Rohr* [1994] study must have been challenging for the sedimented igneous basement where only a fraction of the layer 2A refraction was recorded due to the short maximum offset of 3–3.6 km. Individual interval velocity estimates from *Rohr* [1994] for this deep section of the igneous basement show much greater variability than for the unsedimented basement further supporting this conclusion. The difference between successive layer 2A interval velocity measurements, spatially separated by just a few kilometers, increases with increasing depth to the basement (see Figure 4 in the work of *Rohr* [1994]) reaching >3 km/s. Therefore, it is not surprising that the velocities for the two studies agree within error bounds for the shallow unsedimented igneous crust close to the ridge axis where the data used by *Rohr* [1994] fully image layer 2A event, but do not agree for the deep sedimented section of the igneous basement where the older data lack the far offsets needed to constrain the layer 2A velocities accurately.

[47] The main difference in the data analysis approach between the two studies is that *Rohr* [1994] applied a method that models constant velocity layers and is suited for reflection arrivals, while we used a modeling technique that also allows for vertical gradient velocity layers and is applicable for investigating both reflection and refraction arrivals. This is significant as the layer 2A event is a wide-angle retrograde refraction that for our basement depths does not occur at offsets of <2 km and will therefore stack well at a wide range of NMO velocities. Since for thin layers such as 2A even small variations in the NMO velocity lead to large variations in the derived interval velocity, it is challenging to constrain accurately layer 2A interval velocities based on this approach [e.g., *Harding et al.*, 1993]. Interval velocities derived from stacking velocities for this study show less variation than those from *Rohr* [1994] because we have better constraints from long offsets, as already

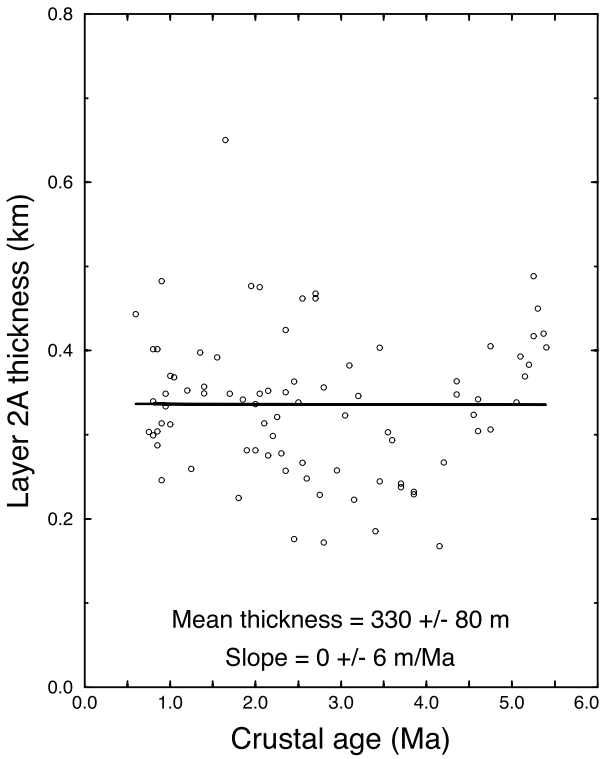

Figure 11. Layer 2A thickness measurements along the sediment blanketed sections of the east Endeavor and east Northern Symmetric transects as a function of oceanic crustal age. Mean thickness and thickness gradient for the plotted data are also shown.

discussed, but also because initial traveltime modeling using vertical gradient velocity layers indicated the need to use consistently the minimum NMO velocity that results in a high-quality layer 2A stack.

5.2.3. Sediment Cover and Layer 2A Thickness

[48] Potential impact of the sealing sedimentary cover on layer 2A thickness is investigated using the same approach as taken in section 5.1.2 to study the relationship between layer 2A thickness and crustal age. Layer 2A thickness estimates from the east Endeavor and east Northern Symmetric ridge flanks, where a generally continuous sediment cover is observed, are plotted in Figure 11 and simple linear regression is applied. The computed thickness gradient of 0 ± 6 m/Ma indicates lack of any systematic trend in layer 2A thickness, which after sediment burial measures on average some 330 ± 80 m. However, layer 2A along the fully sedimented east Endeavor and east Northern Symmetric ridge flanks is on average 100 m thinner than along the sparsely and/or discontinuously sedimented conjugate west flanks and both flanks of the Cleft transect (average thickness of 430 ± 80 m).

[49] The change from a thicker to a thinner layer 2A on the fully sedimented ridge flanks appears to occur within small sections of the seismic transects that extend some 10–20 km and mark the onset of sediment burial. This change in layer 2A thickness is more pronounced on the east Endeavor (CMPs 19000–21000 in Figure 7a) than on the east Northern Symmetric ridge flank (CMPs 21000–23000 in Figure 7b). No further change in layer 2A thickness is observed beyond the onset of full sediment burial region.

[50] We speculate that the change to thinner layer 2A along the sedimented eastern flanks may largely reflect alteration of the lower part of layer 2A with onset of a warmer hydrothermal regime linked to sediment blanketing [*Davis et al.*, 1992] with enhanced precipitation of alteration minerals [*Hunter et al.*, 1999]. Reduction in bulk porosity within layer 2A through infilling of small voids and cracks with mineral precipitates would be expected to have the strongest effect on the high velocity gradient lower section of layer 2A, characterized by lower intrinsic porosities inherited from crustal formation. The closing of thin cracks within this transition zone results in velocity increase that makes the lower part of the high gradient section of layer 2A seismically indistinguishable from layer 2B, essentially leading to a reduction in the layer 2A thickness.

[51] The thinner layer 2A along the fully sediment buried sections of the east Endeavor and east Northern Symmetric flanks may have developed only recently and over a short time period. Sedimentation history in this region is not directly coupled with crustal aging and full sediment burial at the east Endeavor and east Northern Symmetric flanks may be as recent as 0.1 Ma. Hence full burial and therefore more vigorous hydrothermal regime might have affected much of the now blanketed sections of the ridge flanks within a time period that is much shorter than the age of the sediment covered crust, leading to a simultaneous change in layer 2A thickness across a significant crustal age range.

5.3. Impact of Propagator Wakes

[52] Local variations in layer 2A velocity and thickness are evident at more than half of the crossed propagator wakes (Figures 6 and 7). The

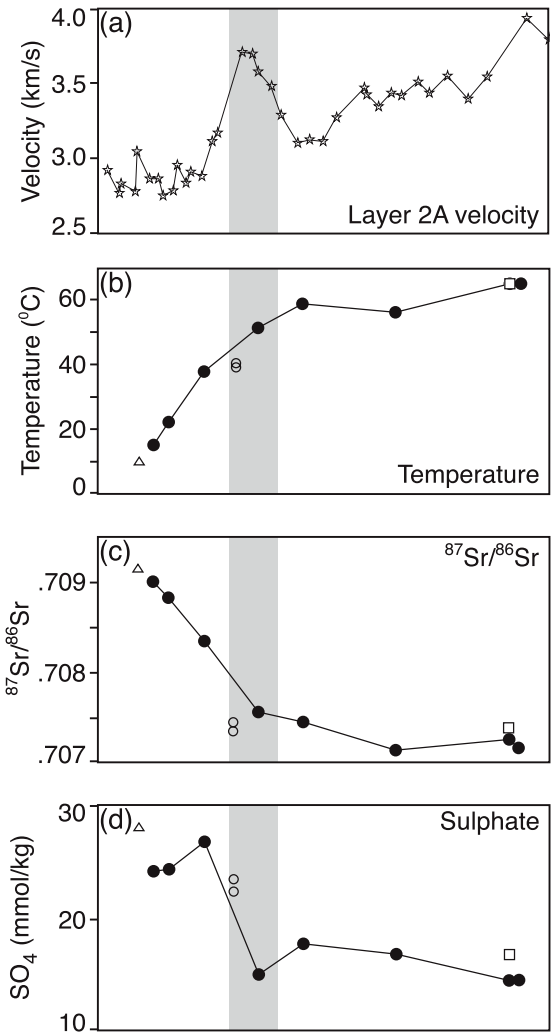

Figure 12. Physical properties of the uppermost oceanic crust and selected chemical properties of the drill hole basement fluids as a function of eastward distance from the Endeavor ridge crest: (a) Subset of seismic velocities shown in Figure 6; (b) temperature; (c) strontium isotopes; (d) sulphate. Triangles indicate seawater (symbol positioned at distance of sediment onlap onto ridge flank); circles indicate basal pore waters from upwelling sites 1030 and 1031; dots indicate basal pore waters from other sites (joined by solid line); squares indicate basement fluid from Site 1026. Plots of chemical properties of basement fluids modified from *Davis et al.* [1997] and *Elderfield et al.* [1999]. Shaded area outlines the location of a propagator wake.

most prominent of these anomalies is found along the east Endeavor transect where a propagator wake is crossed 40–45 km from the ridge axis. Where a local change in layer 2A velocity is identified, it is characterized by increase in the velocity of the high-gradient, lower-layer 2A (0.2–0.5 km/s) and little change in the low-gradient, upper-layer 2A velocity. This leads us to suggest that propagator wakes may represent regions of channelized fluid flow that can potentially have a significant effect on alteration history and basement fluid-flow patterns not previously recognized. Alternatively, the anomalous layer 2A structure could be inherited from the time of crustal accretion [*Bazin et al.*, 2001].

5.4. Correlation With Drill Hole Studies Along the East Endeavor Corridor

[53] Our east flank Endeavor seismic profile is coincident with the borehole transect of Leg 168 of the Ocean Drilling Program (ODP), providing a unique opportunity to constrain inferences from the seismic data on alteration of the shallow oceanic crust. Ten holes along a transect ~120 km long were drilled through the sediment column and into the shallow basement (mostly <10 m), with sediment pore water samples collected to the sediment-basement interface [*Elderfield et al.*, 1999]. Stored samples were later analyzed to examine the conditions of fluid-rock interactions in the low temperature (<150°C) hydrothermal regime that varies from one with open communication with the seawater column to one with very limited communication with the ocean [*Davis et al.*, 1997]. Results of these analyses indicate that the seawater passing through the oceanic crust has reacted with basement rocks [e.g., *Elderfield et al.*, 1999] and alteration minerals in shallow basement rocks indicate a general trend of increasing alteration with distance across the eastern flank from the ridge axis, as well as with depth of sediment burial [*Hunter et al.*, 1999]. These results confirm that the progressive increase in 2A velocities we observe are linked to alteration of the uppermost crust.

[54] In Figure 12, we compare the change in physical properties of the uppermost crust, namely *P* wave velocities from this study, with the change in the strontium isotope ratio and sulphate content of the borehole basement fluids along the east Endeavor ODP transect. On a regional scale, increase in the layer 2A *P* wave velocity correlates well with major changes in these two pore fluid chemical parameters indicative of increased fluid-rock reactions. Other chemical parameters [see *Elderfield et al.*, 1999], not shown in Figure 12, show similar correlation. The majority of geochemical change occurs within the first 30–40 km from the onset of the sedimentary cover, coincident with

the prominent basement scarp ~19 km eastward from the ridge crest. Velocities do not start to change immediately with the onset of sedimentary cover but rather some 5–10 km eastward from this location. Beyond this point velocities, when the effect of the propagator wake is removed, appear to increase approximately monotonously with distance away from the ridge crest.

[55] Notably, the propagator wake is the site of ODP Leg 168 drill holes 1030, 1031, and 1028 (Figures 6 and 7: 1030 and 1031 on the young crust side, 1028 across the age discontinuity on older crust). Basalts sampled at the base of hole 1025 to the west of the wake are vesicular massive ferrobasalts [*Davis et al.*, 1997] and can now be recognized as the Fe-rich basalts often found in proximity to propagating ridge tips. Basement recovery for holes drilled within the wake itself was negligible which could reflect more sheared and fractured basement associated with these structures. The chemical signature of the fluids sampled over the propagator wake show either anomalous values or a major change in spatial gradient. This further supports our suggestion that propagators may locally modify the regional basement fluid flow and could be characterized by a unique alteration history.

6. Conclusions

[56] We described a systematic and uniform approach to extracting upper crustal *P* wave velocity and layer 2A thickness from our 2002 Juan de Fuca MCS data by 1-D traveltime modeling at ~3 km intervals along 300 km long transects crossing the Endeavor, Northern Symmetric, and Cleft ridge segments. For this analysis we constructed 6000 constant offset stack CMP supergathers and selected 300 best suited for 1-D traveltime modeling. To support the traveltime modeling, we first formed coincident seismic reflection images.

[57] Regionally, our results show a direct correlation between an increase in layer 2A velocity and increasing crustal age. However, the identified velocity increase varies across the investigated ridge flanks and supports a first-order effect of full sediment burial on layer 2A evolution. For the flanks blanketed with a continuous sealing sedimentary cover, the velocity increases at about twice the rate observed for ridge flanks with sparse or discontinuous sediment cover (0.24 versus 0.11 km s^{-1}/Ma). Extrapolation of the rate of velocity change with crustal age suggests that on the flanks with continuous sediment cover layer 2A velocity may reach values typical of mature oceanic crust (~4.3 km/s) in <10 Ma. For the sparsely sedimented or sediment barren flanks velocities increase more slowly (~16 Ma to reach ~4.3 km/s). The correlation between layer 2A velocity and sediment cover is likely due to more rapid precipitation of alteration minerals in the porous upper crust as the hydrothermal regime evolves from one dominated by open exchange with the water column to a regime that is effectively closed to seawater exchange by the sealing sedimentary blanket.

[58] The computed ridge-normal thickness gradients show that layer 2A does not systematically thin and disappear in the Juan de Fuca region with increasing crustal age, although the increasing seismic velocities indicate progressive alteration. Layer 2A persists as a region of relatively lower seismic velocities capping the oceanic crust regardless of the presence and type or lack of the sedimentary cover. However, layer 2A along the fully sedimented ridge flanks is on average 100 m thinner than along the sparsely and discontinuously sedimented flanks (330 ± 80 m versus 430 ± 80 m). The transition from thinner to thicker layer 2A appears to take place in the region some 10–20 km wide and centered on the onset of sediment burial. Change in layer 2A thickness beyond the onset of full sediment burial region is not observed.

[59] We speculate that the change to thinner layer 2A along the sedimented eastern flanks is caused by alteration of the lower part of layer 2A with onset of a warmer hydrothermal regime linked to sediment blanketing with enhanced precipitation of alteration minerals. Consequent closing of thin cracks in the low-porosity lowermost layer 2A results in velocity increase that is significant enough to make this section of layer 2A seismically indistinguishable from layer 2B, essentially reducing the layer 2A thickness. The thinner layer 2A along the fully sediment buried sections of the east Endeavor and east Northern Symmetric flanks may have developed only recently and over a short time period. This is possible due to decoupling between the sedimentation history and crustal aging that provides a mechanism for recent full sediment blanketing and simultaneous layer 2A thinning within sedimented crust of different age.

[60] Locally, our results show correlation between the location of propagator wakes and a change in layer 2A thickness and velocity. This indicates that

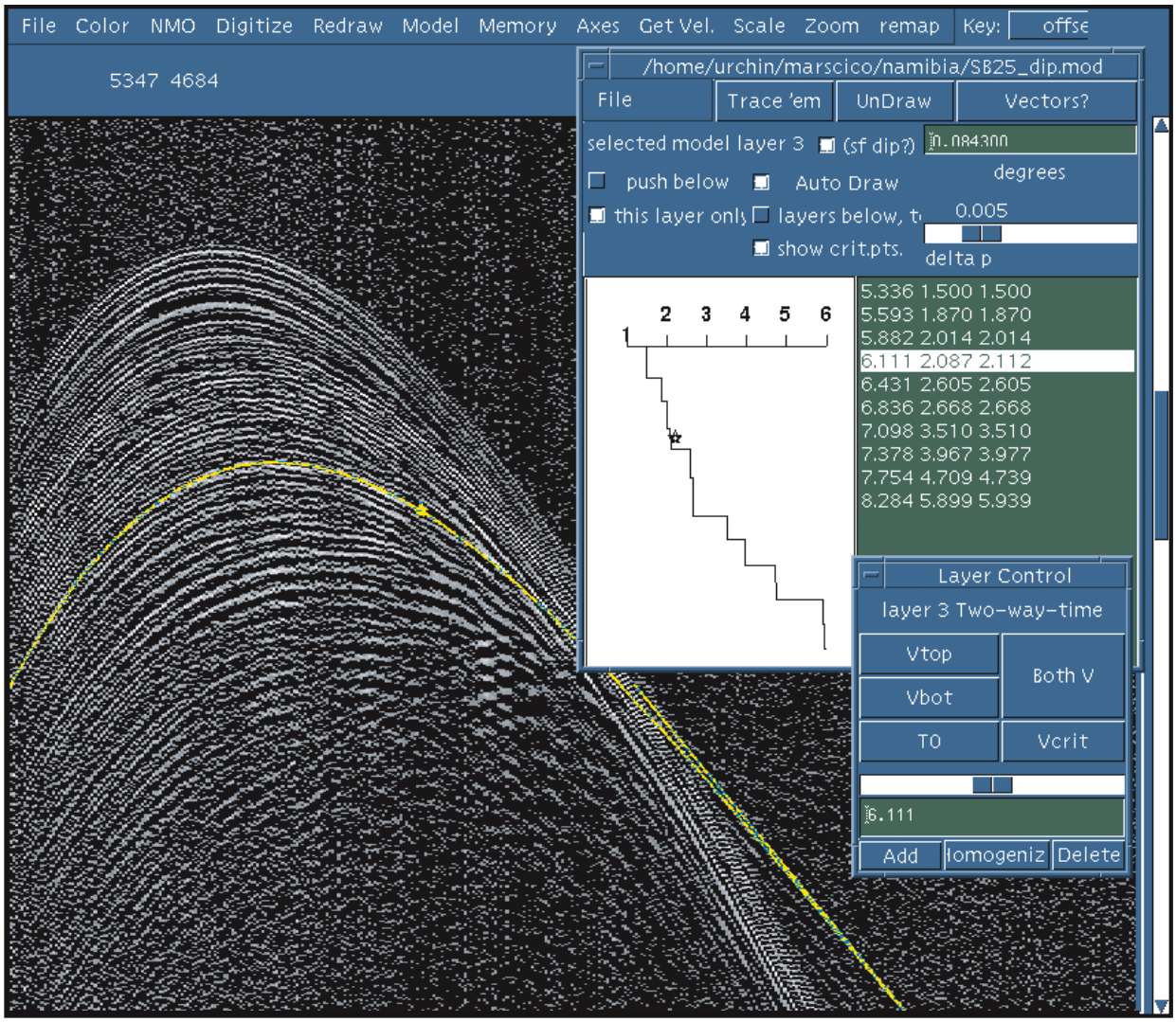

Figure A1. JDseis software main window with various pull down menus and a couple of utility windows open.

either some propagator wakes represent zones of enhanced fluid flow and enhanced precipitation of alteration minerals, or extrusive sections in these areas are formed in a unique way. The chemical signatures of the fluids sampled by ODP/IODP drill holes along the east Endeavor transect support this observation. Other short wavelength variations in 2A structure are evident in our analysis but determining the origin of these anomalies will require application of 2-D analysis techniques, in particular 2-D tomography.

Appendix A: JDseis Software

[61] JDseis is a tool for display and interactive analysis of seismic data (Figure A1), including stacked sections and τ-p and t-x ensembles, where τ is intercept or vertical delay time, p is slowness, t is two-way traveltime, and x is source-receiver offset. One of the most important t-x data image manipulations is the use of a "reducing velocity" ($V_{REDUCTION}$) to apply a linear moveout (LMO) or a deck-of-cards linear time shift:

$$t_{REDUCED} = t_{RECORDED} - x/V_{REDUCTION} \qquad (A1)$$

This time shift greatly improves the visual discrimination of various reflection and refraction branches. During the ray tracing, predicted traveltime arrivals are superimposed upon these images and constantly redrawn as the model is developed and modified.

A1. JDseis Ray Trace Models

[62] In general, distinct, coherent body wave arrivals in MCS data arise from one of three physical processes: precritical reflection, postcritical reflec-

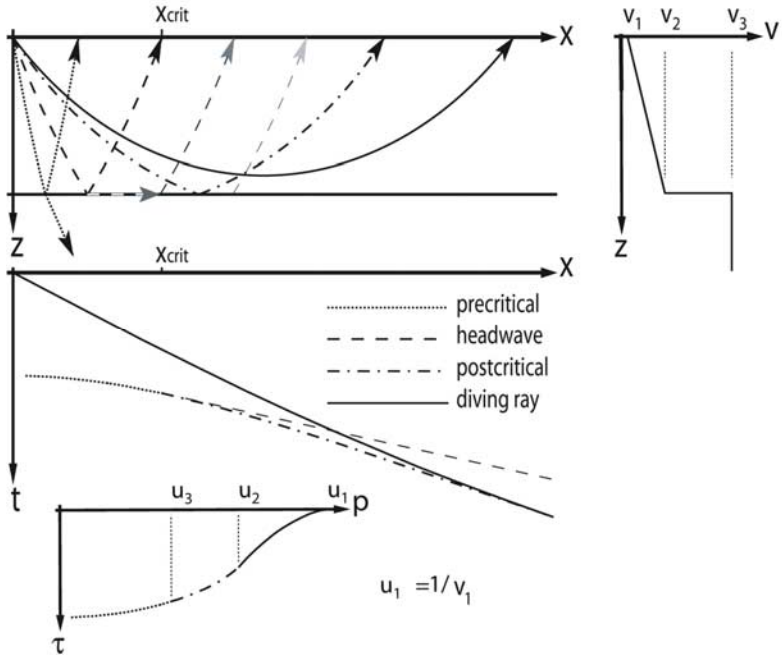

Figure A2. Plot showing seismic arrivals modeled with JDseis. Shown is (top left) a two-layer model with (top right) the velocity structure. The model generates four types of seismic arrivals: precritical reflection, postcritical reflection, head waves, and turning, or diving rays, showing (bottom) these arrivals in t-x and τ-p domain.

tion, and refraction. Two types of refracted arrivals have been used for interpretation: head waves and turning, or diving rays. A head wave arises when a wave intersects a velocity discontinuity at one particular angle (the "critical angle") at which its refraction creates a phase that travels along the discontinuity. Virtually all of the incident energy, however, is reflected upward, the critical reflection. On the other hand, a wave traveling at an angle within a vertical velocity gradient will refract continuously, following a circular path. When these waves are turned enough that they begin to travel upward, they are in fact "totally refracted."

[63] A generalized layer represented by a vertical velocity gradient and a velocity discontinuity at its bottom can generate all four types of arrivals (Figure A2). JDseis models are made up of a stack of such layers, any of which may or may not include a vertical velocity gradient. Analysis is carried out from top down, since the results of each overlying layer affect the raypaths in layers below. When creating a new model, layers are added or inserted as needed, and their two way times and velocities altered to obtain the best fit "by eye" to observed arrivals in the data. As these changes are made, a graphic display of the current model is updated (Figure A1) so that the creation of erroneous and unrealistic layers can be avoided. While modeling gathers along an MCS line, it is most productive to modify existing models from adjacent locations. In this way, horizons can be tracked consistently along the line. Identification of primary arrivals in the data and choice of which arrivals to fit is a crucial step in the analysis, and accuracy depends heavily on the experience of and care taken by the interpreter. Best results are usually attained through working iteratively with groups of records acquired in geologically similar environments. The same arrivals should appear on each record, but due to differences in water depth and other layer thicknesses, the exact position and appearance of various arrivals will differ, making it easier to decide whether or not they in fact exist.

A2. Accuracy

[64] It is difficult to properly quantify the accuracy of any method of velocity analysis. This is due to the great variety in the appearance of the arrivals and in the range of offsets over which they may be observed. The default velocity step used in the JDseis ray tracing is 5 m/s, and when reflected or refracted arrivals can be observed over a significant enough range of offsets, the velocity resolution under ideal circumstances is within this range. This condition is usually met with reflections within homogeneous layers. Postcritically refracted arriv-

als are usually seen within a smaller span of source-receiver offsets, and the velocity resolution may be as high as 10–25 m/s, depending on the vertical velocity gradients.

Acknowledgments

[65] This research was supported by National Science Foundation grants OCE-00-02488, OCE-00-02551, and OCE-00-02600. We are grateful to Captain Mark Landow, Science Officer Joe Stennet, the crew, and the scientific and technical party of the R/V *Maurice Ewing* Cruise 02–07 for their support and help during the data acquisition. We thank R. L. Carlson, G. L. Christeson, and E. E. Davis for their critical reviews.

References

Alt, J. C. (1995), Subseafloor processes in mid-ocean ridge hydrothermal systems, in *Seafloor Hydrothermal Systems: Physical, Chemical, Biological, and Geological Interactions*, *Geophys. Monogr. Ser.*, vol. 91, edited by S. Humphris et al., pp. 85–114, AGU, Washington, D.C.

Barclay, A. H., and W. S. D. Wilcock (2004), Upper crustal seismic velocity structure and microearthquake depths at the Endeavour Segment, Juan de Fuca Ridge, *Geochem. Geophys. Geosyst.*, *5*, Q01004, doi:10.1029/2003GC000604.

Bazin, S., et al. (2001), Three-dimensional shallow crustal emplacement at the 9°03′N overlapping spreading center on the East Pacific Rise: Correlations between magnetization and tomographic images, *J. Geophys. Res.*, *106*, 16,101–16,117, doi:10.1029/2001JB000371.

Blacic, T., G. Ito, J. P. Canales, R. S. Detrick, and J. M. Sinton (2004), Constructing the crust along the Galapagos Spreading Center 91.3°–95.5°W: Correlation of seismic layer 2A with axial magma lens and topographic characteristics, *J. Geophys. Res.*, *109*, B10310, doi:10.1029/2004JB003066.

Canales, J. P., R. S. Detrick, S. M. Carbotte, G. M. Kent, J. B. Diebold, A. J. Harding, J. M. Babcock, M. R. Nedimović, and E. M. van Ark (2005), Upper crustal structure and axial topography at intermediate-spreading ridges: Seismic constraints from the southern Juan de Fuca Ridge, *J. Geophys. Res.*, *110*, B12104, doi:10.1029/2005JB003630.

Canales, J. P., S. C. Singh, R. S. Detrick, S. M. Carbotte, A. J. Harding, G. M. Kent, J. B. Diebold, J. Babcock, and M. R. Nedimović (2006), Seismic evidence for variations in axial magma chamber properties along the southern Juan de Fuca Ridge, *Earth Planet. Sci. Lett.*, *246*, 353–366, doi:10.1016/j.epsl.2006.04.032.

Carbotte, S. M., G. Ponce-Correa, and A. Solomon (2000), Evaluation of morphological indicators of magma supply and segmentation from a seismic reflection study of the EPR 15°30′–17°N, *J. Geophys. Res.*, *105*, 2737–2759, doi:10.1029/1999JB900245.

Carbotte, S. M., R. S. Detrick, A. J. Harding, J. P. Canales, J. Babcock, G. M. Kent, E. M. Van Ark, M. R. Nedimović, and J. B. Diebold (2006), Rift topography linked to magmatism at the intermediate spreading Juan de Fuca Ridge, *Geology*, *34*, 209–212, doi:10.1130/G21969.1.

Carbotte, S. M., M. R. Nedimović, J. P. Canales, G. M. Kent, and A. J. Harding (2008), Variable crustal structure along the Juan de Fuca Ridge: Influence of on-axis hotspots and absolute plate motions, *Geochem. Geophys. Geosyst.*, *9*, Q08001, doi:10.1029/2007GC001922.

Carlson, R. L. (1998), Seismic velocities of the uppermost igneous crust: Age dependence and the fate of layer 2A, *J. Geophys. Res.*, *103*, 7069–7077, doi:10.1029/97JB03577.

Carlson, R. L. (2004), Seismic properties of layer 2A at 11 Ma: Results of a vertical seismic profile at Ocean Drilling Program Site 1243, *Geophys. Res. Lett.*, *31*, L17601, doi:10.1029/2004GL020598.

Christeson, G. L., G. M. Purdy, and K. M. M. Rohr (1993), Structure of the Northern Symmetrical Segment of the Juan de Fuca Ridge, *Mar. Geophys. Res.*, *15*, 219–240, doi:10.1007/BF01204234.

Christeson, G. L., G. M. Purdy, and G. J. Fryer (1994), Seismic constraints on shallow crustal emplacement processes at the fast spreading East Pacific Rise, *J. Geophys. Res.*, *99*, 17,957–17,973, doi:10.1029/94JB01252.

Christeson, G. L., K. D. McIntosh, and J. A. Karson (2007), Inconsistent correlation of seismic layer 2a and lava layer thickness in oceanic crust, *Nature*, *445*, 418–421, doi:10.1038/nature05517.

Collier, J. S., and S. C. Singh (1998), Poisson's ratio structure of young oceanic crust, *J. Geophys. Res.*, *103*, 20,981–20,996, doi:10.1029/98JB01980.

Cudrak, C. F., and R. M. Clowes (1993), Crustal structure of Endeavour ridge segment, Juan de Fuca ridge, from a detailed seismic refraction survey, *J. Geophys. Res.*, *98*, 6329–6349, doi:10.1029/92JB02860.

Davis, E. E., and J. L. Karsten (1986), On the cause of the asymmetric distribution of seamounts about the Juan de Fuca Ridge; ridge-crest migration over a heterogeneous asthenosphere, *Earth Planet. Sci. Lett.*, *79*, 385–396, doi:10.1016/0012-821X(86)90194-9.

Davis, E. E., et al. (1992), Flankflux, An experiment to study the nature of hydrothermal circulation in young oceanic crust, *Can. J. Earth Sci.*, *29*, 925–952.

Davis, E. E., A. T. Fisher, and J. V. Firth (1997), The Shipboard Scientific Party, Hydrothermal circulation in the oceanic crust: Eastern flank of the Juan de Fuca Ridge, *Proc. Ocean Drill. Program Initial Rep.*, *168A*, 1–470.

Diebold, J. B., and P. L. Stoffa (1981), The traveltime equation, tau-p mapping and inversion of common midpoint data, *Geophysics*, *46*, 238–254, doi:10.1190/1.1441196.

Dix, C. H. (1955), Seismic velocities from surface measurements, *Geophysics*, *20*, 68–86, doi:10.1190/1.1438126.

Elderfield, H., C. G. Wheat, M. J. Mottl, C. Monnin, and B. Spiro (1999), Fluid and geochemical transport through oceanic crust: A transect across the eastern flank of the Juan de Fuca Ridge, *Earth Planet. Sci. Lett.*, *172*, 151–165, doi:10.1016/S0012-821X(99)00191-0.

Fisher, A. T., and K. Becker (1995), Correlation between seafloor heat flow and basement relief: Observational and numerical examples and implications for upper crustal permeability, *J. Geophys. Res.*, *100*, 12,641–12,657, doi:10.1029/95JB00315.

Fisher, A. T., et al. (2003), Hydrothermal recharge and discharge across 50 km guided by seamounts on a young ridge flank, *Nature*, *421*, 618–621, doi:10.1038/nature01352.

Grevemeyer, I., and A. Bartetzko (2004), Hydrothermal aging of ocenic crust; inferences from seismic refraction and borehole studies, in *Hydrogeology of the Oceanic Lithosphere*, edited by E. E. Davis and H. Elderfield, pp. 128–150, Cambridge Univ. Press, New York.

Grevemeyer, I., and W. Weigel (1996), Seismic velocities of the uppermost igneous crust versus age, *Geophys. J. Int.*, *124*, 631–635, doi:10.1111/j.1365-246X.1996.tb07041.x.

Grevemeyer, I., and W. Weigel (1997), Increase of seismic velocities in upper oceanic crust: The "superfast" spreading

East Pacific Rise at 14°14′S, *Geophys. Res. Lett.*, *24*, 217–220, doi:10.1029/96GL04005.

Grevemeyer, I., N. Kaul, H. Villinger, and W. Weigel (1999), Hydrothermal activity and the evolution of the seismic properties of the upper oceanic crust, *J. Geophys. Res.*, *104*, 5069–5079, doi:10.1029/1998JB900096.

Harding, A. J., G. M. Kent, and J. A. Orcutt (1993), A multichannel eismic investigation of upper crustal structure at 9°N on the East Pacific Rise: Implications for crustal accretion, *J. Geophys. Res.*, *98*, 13,925–13,944, doi:10.1029/93JB00886.

Herron, T. J. (1982), Lava flow layer-East Pacific Rise, *Geophys. Res. Lett.*, *9*, 17–20, doi:10.1029/GL009i001p00017.

Houtz, R., and J. Ewing (1976), Upper crustal structure as a function of plate age, *J. Geophys. Res.*, *81*, 2490–2498, doi:10.1029/JB081i014p02490.

Hunter, A. G., P. D. Kempton, and P. Greenwood (1999), Low-temperature fluid-rock interaction-an isotopic and mineralogical perspective of upper crustal evolution, eastern flank of the Juan de Fuca Ridge (JdFR), ODP Leg 168, *Chem. Geol.*, *155*, 3–28, doi:10.1016/S0009-2541(98)00138-7.

Hussenoeder, S. A., R. S. Detrick, G. M. Kent, H. Schouten, and A. J. Harding (2002), Fine-scale seismic structure of young upper crust at 17°20′S on the fast spreading East Pacific Rise, *J. Geophys. Res.*, *107*(B8), 2158, doi:10.1029/2001JB001688.

Jacobson, R. S. (1992), Impact of crustal evolution on changes of the seismic properties of the uppermost ocean crust, *Rev. Geophys.*, *30*, 23–42, doi:10.1029/91RG02811.

Johnson, H. P., K. Becker, and R. Von Herzen (1993), Near-axis heat flow measurements on the northern Juan de Fuca Ridge: Implications for fluid circulation in oceanic crust, *Geophys. Res. Lett.*, *20*, 1875–1878, doi:10.1029/93GL00734.

Kennett, B. L. N., and J. A. Orcutt (1976), Comparison of travel time inversions for marine refraction profiles, *J. Geophys. Res.*, *81*, 4061–4070, doi:10.1029/JB081i023p04061.

Kent, G. M., A. J. Harding, J. A. Orcutt, R. S. Detrick, J. C. Mutter, and P. Buhl (1994), Uniform accretion of oceanic crust south of the Garrett transform at 14°15′S on the East Pacific Rise, *J. Geophys. Res.*, *99*, 9097–9116, doi:10.1029/93JB02872.

Langseth, M. G., M. J. Mottl, M. A. Hobart, and A. Fisher (1988), The distribution of geothermal and geochemical gradients near Site 501/504: Implications for hydrothermal circulation in the oceanic crust, *Proc. Ocean Drill. Program Initial Rep.*, *111*, 23–32.

McClain, J. S., and C. A. Atallah (1985), The structure of young oceanic crust bear a very fast spreading ridge, *Geophys. Res. Lett.*, *12*, 689–692, doi:10.1029/GL012i010p00689.

McClain, J. S., and B. T. R. Lewis (1982), Geophysical evidence for the absence of a crustal magma chamber under the Northern Juan de Fuca Ridge: A contrast with ROSE results, *J. Geophys. Res.*, *87*, 8477–8489, doi:10.1029/JB087iB10p08477.

McClymont, A. F., and R. M. Clowes (2005), Anomalous lithospheric structure of Northern Juan de Fuca plate-a consequence of oceanic rift propagation?, *Tectonophysics*, *406*, 213–231, doi:10.1016/j.tecto.2005.05.026.

McDonald, M. A., J. A. Hildebrand, and S. C. Webb (1994), Seismic structure and anisotropy of the Juan de Fuca Ridge at 45°N, *J. Geophys. Res.*, *99*, 4857–4874, doi:10.1029/93JB02801.

Minshull, T. A., R. S. White, J. C. Mutter, P. Buhl, R. S. Detrick, C. A. Williams, and E. Morris (1991), Crustal structure at the Blake Spur Fracture Zone from expanding spread profiles, *J. Geophys. Res.*, *96*, 9955–9984, doi:10.1029/91JB00431.

Nedimović, M. R., R. D. Hyndman, K. Ramachandran, and G. D. Spence (2003), Reflection signature of seismic and aseismic slip on the northern Cascadia subduction interface, *Nature*, *424*, 416–420, doi:10.1038/nature01840.

Nedimović, M. R., S. M. Carbotte, A. J. Harding, R. S. Detrick, J. P. Canales, G. M. Kent, M. Tischer, J. B. Diebold, and J. M. Babcock (2005), Frozen subcrustal magma lenses, *Nature*, *436*, 1149–1152, doi:10.1038/nature03944.

Purdy, G. M. (1987), New observations of the shallow seismic structure of young oceanic crust, *J. Geophys. Res.*, *92*, 9351–9362, doi:10.1029/JB092iB09p09351.

Purdy, G. M., and J. Ewing (1986), Seismic structure of the ocean crust, in *The Geology of North America*, vol. M, *The Western North Atlantic Region*, edited by P. R. Vogt and B. E. Tucholke, pp. 313–370, Geol. Soc. of Am., Boulder, Colo.

Raitt, R. W. (1963), The crustal rocks, in *The Sea*, vol. 3, *The Earth Beneath the Sea History*, edited by M. N. Hill, pp. 85–102, Wiley-Interscience, New York.

Rohr, K. M. M. (1994), Increase of seismic velocities in upper oceanic crust and hydrothermal circulation in the Juan de Fuca plate, *Geophys. Res. Lett.*, *21*, 2163–2166, doi:10.1029/94GL01913.

Stephen, R. A., and A. J. Harding (1983), Travel time analysis of borehole seismic data, *J. Geophys. Res.*, *88*, 8289–8298, doi:10.1029/JB088iB10p08289.

Talwani, M., C. C. Windisch, and M. G. Langseth (1971), Reykjanes ridge crest: A detailed geophysical study, *J. Geophys. Res.*, *76*, 473–517, doi:10.1029/JB076i002p00473.

Van Ark, E. M., R. S. Detrick, J. P. Canales, S. Carbotte, A. J. Harding, G. M. Kent, M. R. Nedimović, W. S. D. Wilcock, J. B. Diebold, and J. M. Babcock (2007), Seismic structure of the Endeavour segment Juan de Fuca Ridge: Correlations with seismicity, faulting and hydrothermal activity, *J. Geophys. Res.*, *112*, B02401, doi:10.1029/2005JB004210.

Vera, E. E., and J. B. Diebold (1994), Seismic imaging of oceanic layer 2A between 9°30′N and 10°N on the East Pacific Rise from two-ship wide-aperture profiles, *J. Geophys. Res.*, *99*, 3031–3041, doi:10.1029/93JB02107.

Vera, E. E., J. C. Mutter, P. Buhl, J. A. Orcutt, A. J. Harding, M. E. Kappus, R. S. Detrick, and T. M. Brocher (1990), The structure of 0- to 0.2-m.y.-old oceanic crust at 9°N on the East Pacific Rise from expanded spread profiles, *J. Geophys. Res.*, *95*, 15,529–15,556, doi:10.1029/JB095iB10p15529.

Wang, K., J. He, and E. E. Davis (1997), Influence of basement topography on hydrothermal circulation in sediment-buried igneous oceanic crust, *Earth Planet. Sci. Lett.*, *146*, 151–164, doi:10.1016/S0012-821X(96)00213-0.

Wheat, G. C., and M. J. Mottl (1994), Hydrothermal circulation, Juan de Fuca Ridge eastern flank: Factors controlling basement water composition, *J. Geophys. Res.*, *99*, 3067–3080, doi:10.1029/93JB01612.

Whitmarsh, R. B. (1978), Seismic refraction studies of upper igneous crust in North Atlantic and porosity estimates for layer 2, *Earth Planet. Sci. Lett.*, *37*, 451–464, doi:10.1016/0012-821X(78)90061-4.

Wilkens, R. H., G. J. Fryer, and J. Karsten (1991), Evolution of porosity and seismic structure of upper oceanic crust: Importance of aspect ratios, *J. Geophys. Res.*, *96*, 17,981–17,995, doi:10.1029/91JB01454.

Wilson, D. S. (1988), Tectonic history of the Juan de Fuca ridge over the last 40 million years, *J. Geophys. Res.*, *93*, 11,863–11,876, doi:10.1029/JB093iB10p11863.

Wilson, D. S. (1993), Confidence intervals for motion and deformation of the Juan de Fuca plate, *J. Geophys. Res.*, *98*, 16,053–16,071, doi:10.1029/93JB01227.